



저작자표시-비영리-변경금지 2.0 대한민국

이용자는 아래의 조건을 따르는 경우에 한하여 자유롭게

- 이 저작물을 복제, 배포, 전송, 전시, 공연 및 방송할 수 있습니다.

다음과 같은 조건을 따라야 합니다:



저작자표시. 귀하는 원저작자를 표시하여야 합니다.



비영리. 귀하는 이 저작물을 영리 목적으로 이용할 수 없습니다.



변경금지. 귀하는 이 저작물을 개작, 변형 또는 가공할 수 없습니다.

- 귀하는, 이 저작물의 재이용이나 배포의 경우, 이 저작물에 적용된 이용허락조건을 명확하게 나타내어야 합니다.
- 저작권자로부터 별도의 허가를 받으면 이러한 조건들은 적용되지 않습니다.

저작권법에 따른 이용자의 권리는 위의 내용에 의하여 영향을 받지 않습니다.

이것은 [이용허락규약\(Legal Code\)](#)을 이해하기 쉽게 요약한 것입니다.

[Disclaimer](#)

Unraveling the roles of extrinsic factors in cellular plasticity and heterogeneity of ameloblastoma

Shujin Li

Department of Applied Life Science
Graduate School, Yonsei University

**Unraveling the roles of extrinsic factors in
cellular plasticity and heterogeneity of
ameloblastoma**

Directed by Professor: Han-Sung Jung

The Doctoral Dissertation

Submitted to the Department of Applied Life
Science

The Graduate School of Yonsei University in
partial fulfillment of the requirement for the
degree of Ph.D. in Dental Science

Shujin Li

February 2024

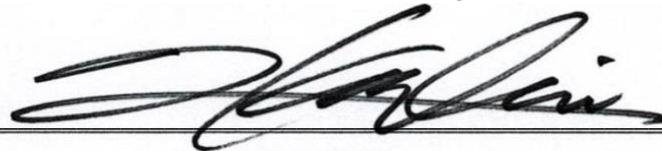
**This certifies that the Doctoral Dissertation of
Shujin Li is approved.**



Han-Sung Jung



Na-Young Song



Jong-Min Lee



Jae-Young Kim



Yoon Jeong Choi

The Graduate School

Yonsei University

December 2023

TABLE OF CONTENTS

LIST OF FIGURES	iii
LIST OF ABBREVIATIONS	iv
ABSTRACT	v
I. GENERAL INTRODUCTION	1
1. Hallmarks of cancer	1
2. Heterogeneity and cellular plasticity of cancer	3
3. Intrinsic and extrinsic factors	5
4. Current understanding of odontogenic tumors	8
5. Aim and objectives	15
II. MATERIALS AND METHODS	16
1. Tissue specimens and processing	16
1.1 Patient tumor samples	16
1.2 Cell and organoid cultures	16
1.3 Construction of pCDH-CACNA1C overexpression vector	18
1.4 Lentivirus production by transfecting HEK 293T cells	18
1.5 Knockdown CACNA1C in AM cells	19
2. Bulk RNA sequencing and analysis	19
3. Histology and immunofluorescence	20
4. Real-time quantitative polymerase chain reaction (RT-qPCR)	21
5. Nucleus/cytoplasm fractionation and Western blot	22
6. Intracellular calcium imaging	23
7. Organoid-forming assays	23
8. Image quantification and statistical analysis	24
III. SECTION 1: Unraveled roles of Cav1.2 in cell stemness and proliferation	25
1. Introduction	25
1.1 Role of calcium signaling in cellular functions	25
1.2 Calcium toolkit: channel, exchanger, and pump in CSCs	26
1.3 Voltage-gated calcium channel in CSCs	26
2. Results	28
2.1 Transcriptome profiling of odontogenic tumors	28
2.2 Cav1.2 is localized in the filopodia tip of patient-derived AM cells	34
2.3 Dynamic Ca ²⁺ influx in pAM cells via Cav1.2	34

2.3 Cav1.2-dependent Ca ²⁺ /NFATc1 signaling coupled with cell proliferation.....	37
2.4 Function of Cav1.2 in maintaining of Wnt/ β -catenin activity.....	41
3. Discussion.....	44
IV. SECTION 2: Ameloblastoma modifies tumor microenvironment for enhancing invasiveness by altering collagen alignment	48
1. Introduction.....	48
2. Results.....	49
2.1 Differences in the tumor microenvironment between AM and OKC	49
2.2 AM and OKC tumoroid formation in different ECM conditions	55
3. Discussion.....	58
V. CONCLUSIONS AND FUTURE PROSPECTS.....	61
1. Conclusions	61
2. Future prospects	62
VI. REFERENCE	63
ABSTRACT IN KOREAN.....	67
PUBLICATION LIST	69

LIST OF FIGURES

Figure 1. Hallmarks of cancer.	6
Figure 2. Molecular mechanism of plasticity.	7
Figure 3. Origin of ameloblastoma.	11
Figure 4. Genetic mutation in ameloblastoma.	12
Figure 5. Enrichment of calcium signal-related GO in AM.	30
Figure 6. Visualization of differentially expressed genes between AM and OKC	31
Figure 7. Transcriptomic and histological differences between AM and OKC.	32
Figure 8. Cav1.2 expression pattern in pAM and pOKC cells.	35
Figure 9. Ca²⁺ influx mediated by L-type VGCC in pAM cells.	36
Figure 10. Ca²⁺ influx increased in CACNA1C-overexpressed pAM cells.	39
Figure 11. PCNA⁺ cells increased in CACNA1C-overexpressed pAM tumoroid.	40
Figure 13. Cav1.2 maintained Wnt/β-catenin signaling activity in pAM tumoroids. ...	43
Figure 14. Cav1.2-mediated calcium signaling in AM.	47
Figure 15. Transcriptomic and histopathologic differences in the TME of AM and OKC.	52
Figure 16. Transcriptomic profiling of AM and OKC.	53
Figure 17. Unique collagen fiber distribution in each stroma of the AM and OKC. ...	54
Figure 18. Tumoroid formation by AM and OKC under different ECM conditions. .	56
Figure 19. RT-qPCR of secreting collagen remodeling molecules.	57
Figure 20. Tumor microenvironments in odontogenic tumors.	60

LIST OF ABBREVIATIONS

Ameloblastoma (AM)
Basement membrane (BM)
Cytomegalovirus (CMV)
Cancer stem cells (CSCs)
Cytokeratin 10 (CK10)
Cytokeratin 14 (CK14)
Collagen I (Col I)
Collagen IV (Col IV)
Cancer-associated-fibroblast (CAF)
Extracellular matrix (ECM)
Epithelial rests of Malassez (ERM)
Epithelial to mesenchymal transition (EMT)
Fibroblast activation protein (FAP)
Gene ontology (GO)
Lysyl oxidase like-2 (LOXL2)
Odontogenic keratocyst (OKC)
Overexpression (OE)
Principal component analysis (PCA)
Patient-derived ameloblastoma (pAM)
Patient-derived odontogenic keratocyst (pOKC)
Tumor microenvironment (TME)
TO-PRO-3 (TP3)
Voltage-Operated Channels (VOCs)
Voltage-gated calcium channels (VGCCs)
Verapamil (VPM)

ABSTRACT

Unraveling the roles of extrinsic factors in cellular plasticity and heterogeneity of ameloblastoma

Shujin Li

Department of Applied Life Science, The Graduate School, Yonsei University

(Directed by Professor Han-Sung Jung)

Cancer initiation and progression, along with the development and sustenance of intratumoral heterogeneity, are closely linked to the fundamental concept of plasticity. However, the intricate nature of cancer and the heterogeneity within the cancer population pose challenges to the advancement of anti-cancer therapies. The extrinsic factors within the tumor microenvironment (TME) function as extracellular inputs to the cancer cell system, continuously transitioning the cell state to acquire cellular plasticity and contributing to the heterogeneity of cancer. Ameloblastoma, a representative odontogenic epithelial tumor was introduced as a model system to study the relationship between extrinsic factors from TME and the heterogeneity of cancer cells. In the present study, the roles of two typical extrinsic factors (high calcium ion environment and collagen-rich extracellular matrix) from ameloblastoma TME were investigated in detail. Cav1.2 (L-type voltage-gated calcium channel) was dominantly expressed in the plasma membrane of ameloblastoma cells. This intensive, frequent extracellular calcium signaling activated the calcium signal-related transcription factor NFATC1 contributing to the transition of ameloblastoma cells to the

proliferative state. The Cav1.2-mediated calcium signal triggers the nuclei translocation of β -catenin within the non-classical Wnt signaling pathway. Subsequently, the augmentation of Wnt signaling activity contributed to the maintenance of cancer stemness, which is essential for establishing intratumoral heterogeneity during the progression of ameloblastoma. The widely distributed, well-aligned collagen bundles constituted a stiffened ECM in the ameloblastoma and provided a pro-invasive tract for tumor expansion and metastasis. The alignment of collagen fibers functions as an extrinsic factor to provide stimulation from extracellular environments for the acquisition of plasticity and, eventually, the attainment of cancer heterogeneity in ameloblastoma. Targeting Cav1.2 or modifying the distribution of collagen fibers in ameloblastoma (evenly in other cancers that harbored similar environmental cues in the tumor microenvironment) will be a viable option for providing a combination treatment with intrinsic factor inhibitors. However, the precise mechanistic network responsible for the interaction between cancer cells and the surrounding TME should be evaluated in the multiple model system in future studies to determine the therapeutic effects of combining these intrinsic and extrinsic factors.

Key words: Heterogeneity; Cellular plasticity; Tumor microenvironment; Cav1.2; Collagen-rich ECM; Ameloblastoma

I. GENERAL INTRODUCTION

1. Hallmarks of cancer

What is cancer? As defined by the National Cancer Institute of the U.S., cancer can be succinctly outlined as a disease in normal cells of specific tissues that undergo uncontrolled growth, proliferation, and dissemination to other regions of the body. However, cancer is daunting in the breadth and scope of its diversity, spanning genetics, cell and tissue biology, pathology, and its response to therapy (Hanahan 2022). Carcinogenesis, also called oncogenesis or tumorigenesis, is a multistep process accompanied by multiple genetic changes that propel the gradual conversion of ordinary cells into highly malignant counterparts. More specifically, cells evolve progressively from normalcy through premalignant states into invasive cancers.

Indeed, the development of tumors collectively adheres to a process formally analogous to Darwinian evolution (Nowell 1976). Over the past 50 years, a vast and intricate body of work has revealed that the genomes of cancer cells are invariably altered at multiple sites, by point mutations and changes in chromosome complement. The mutational discoveries, including the activation of oncogenes by dominant gain of function mutations or the inhibition of tumor suppressor genes with recessive loss of function mutations, contribute toward understanding cancer at both the molecular and cellular levels. Meanwhile, some argue for further exploring the origin and treatment of cancer, it is inevitable that the scientific literature, which is already immensely intricate, will continue to gain additional layers of complexity.

However, cancer research is transitioning into a more systematic science. The intricacies of cancer described in the laboratory and clinical settings are gradually becoming more

comprehensible through a few sets of fundamental principles at a conceptual level. In 2000, Douglas Hanahan and Robert A. Weinberg initially introduced the conceptual framework known as the "**Hallmarks of Cancer**", which aimed to distill the extensive complexity of cancer phenotypes and genotypes into a preliminary set of fundamental principles. Primarily, six distinctive and complementary capabilities were indicated to facilitate tumor growth and metastatic dissemination—sustaining proliferative signaling, evading growth suppressors, resisting cell death, enabling replicative immortality, inducing angiogenesis, and activating invasion and metastasis—that provide a solid foundation for comprehending the biology of cancer (Hanahan & Weinberg 2000). Over the ensuing decade, this concept had been consolidated and expanded, and two “emerging hallmarks” were proposed: deregulating cellular energetics and avoiding immune destruction.

Furthermore, a consensus emerged regarding the foundation of these hallmarks, which comprises two enabling characteristics. Most prominent is the emergence of genomic instability in cancer cells, resulting in random mutations, including chromosomal rearrangements. The second enabling characteristic involves the inflammatory state of premalignant and malignant lesions driven by immune cells, some of which contribute to tumor progression through various mechanisms (Hanahan & Weinberg 2011). Thus 11 years later, a discrete hallmark capability involving phenotypic plasticity and disrupted differentiation has been raised. Moreover, senescent cells, originating from multiple sources, are also included in these emerging hallmarks. Meanwhile, non-mutational epigenetic reprogramming and polymorphic microbiomes constituted distinctive enabling characteristics that facilitate the acquisition of hallmark capabilities (Hanahan & Weinberg 2011). This conceptual framework (Fig. 1) promoted the rationalization of the intricate

phenotypes observed in various human tumor types and variants, elucidating them through a shared set of fundamental cellular parameters.

2. Heterogeneity and cellular plasticity of cancer

Previously, most cancer research and therapeutic decisions were conducted on a patient cohort-wide scale. Conventional treatment approaches primarily focus on a single receptor or pathway, thereby aiming to treating cancer as a homogeneous disease. Even in current precision medicine programs, which involve the genetic analysis of individual patient tumors to pinpoint the optimal targeted therapy, the detectability of the targeted variant was solely highlighted, disregarding the consideration that it is being expressed by numerous cells (Lih et al., 2017). This therapeutic strategy might prove ineffective for several reasons: (i) The variant is not essential for propelling tumor growth; (ii) it is not expressed in cell populations that promote tumor development; (iii) specific cell populations harbor additional mutations that drive or confer resistance; (iv) factors influencing tumor growth, viability, or resistance are encoded at the non-genetic level. Collectively, the barrier to cancer treatment, primarily arises from the heterogeneity of cancer.

Heterogeneity is universal in cancer and manifests as morphological differences between cancer cell populations, distinct genetic profiles, or phenotypic properties, each with the potential to contribute to progression, metastasis, and drug resistance variably (Welch 2016). The heterogeneity of cancer cells emerges through various mechanisms. One theory posits that the acquisition of subclones with increased genetic diversity and distinct tumor genotypes over time is due to the stochastic accumulation of mutations through genomic instability (McGranahan & Swanton 2015). Additionally, cellular differentiation is another theory in the heterogeneity of cancer biology. Cancers exhibit a hierarchical organization

with a population resembling cancer stem cells (CSCs), sustaining tumor growth through processes of self-renewal and differentiation (Kreso & Dick 2014). Growing evidence suggests that the tumor microenvironment (TME) contributes to intratumor heterogeneity by exerting diverse selective pressures in specific tumor areas (Black et al., 2015, Quail & Joyce 2013, Widmer et al., 2013). These models are not mutually exclusive and cooperate to generate an intricately characterized system by dynamic heterogeneity arising from different genetic, epigenetic, transcriptomic, proteomic, and functional properties within various cancer cell populations.

The interpretation of cancer heterogeneity could commence from the perspective of cellular plasticity. As a fundamental characteristic of biological systems, plasticity refers to the capacity of cells to assume new states or phenotypes through the differentiation process (Torborg et al., 2022). The pivotal role of cellular plasticity during embryonic development and tissue regeneration has been studied for decades. However, the critical role of plasticity in the cancer initiation and progression, the acquisition of adaptability for therapeutic inhibition, and the emergence and perpetuation of intratumoral heterogeneity remain poorly understood. Suppose the heterogeneity can be briefly described as a diversity of the cell state, then the plasticity can be considered the adaptability or flexibility to transition from one state to another. Thus, the numerous studies in cancer biology underscore that heterogeneity poses a significant obstacle to cancer treatment. **Cellular plasticity**, identified as the primary force influencing alterations in cell states, raises the question: What is the principal driver of cellular plasticity in cancer?

3. Intrinsic and extrinsic factors

Previously, cancer cell plasticity was thought to arise solely from the accumulation of aberrant mutations in tumor cells. However, an accumulation of evidence indicates that cancer heterogeneity is also shaped by the nature of cancer's microenvironmental constitution, and its stromal cell proportions or activation states (Hanahan & Coussens 2012).

Cellular plasticity is a sum of the cellular **intrinsic** epigenetic and biochemical conditions (system), and the **extrinsic** signals (inputs). The intrinsic cellular and molecular features could be include epigenetic mechanisms, such as DNA methylation, mutational state, histone modifications, such as acetylation and methylation, and chromatin accessibility differences (Pihan & Doxsey 2003). Indeed, the chromatin accessibility changes associated with wound healing illustrated increased plasticity and cooperated with tumor initiation (Concepcion et al., 2022). The extrinsic factors contain various environmental inputs, such as intercellular signaling between cancer and stromal cells, a complex meshwork of extracellular matrix (ECM) proteins, physical and chemical environment conditions (pH, Ca²⁺, and osmolarity), metabolic niche, hypoxia, and immune response (Fig. 2). Hence, it could be speculated that enhancing the effectiveness of anti-cancer therapy by targeting cellular plasticity may entail the modification of either the "system" itself or the external "inputs" that define the plastic cell states. Another strategy involves directing cytotoxicity towards highly plastic cancer cells by focusing on specific cell surface markers.

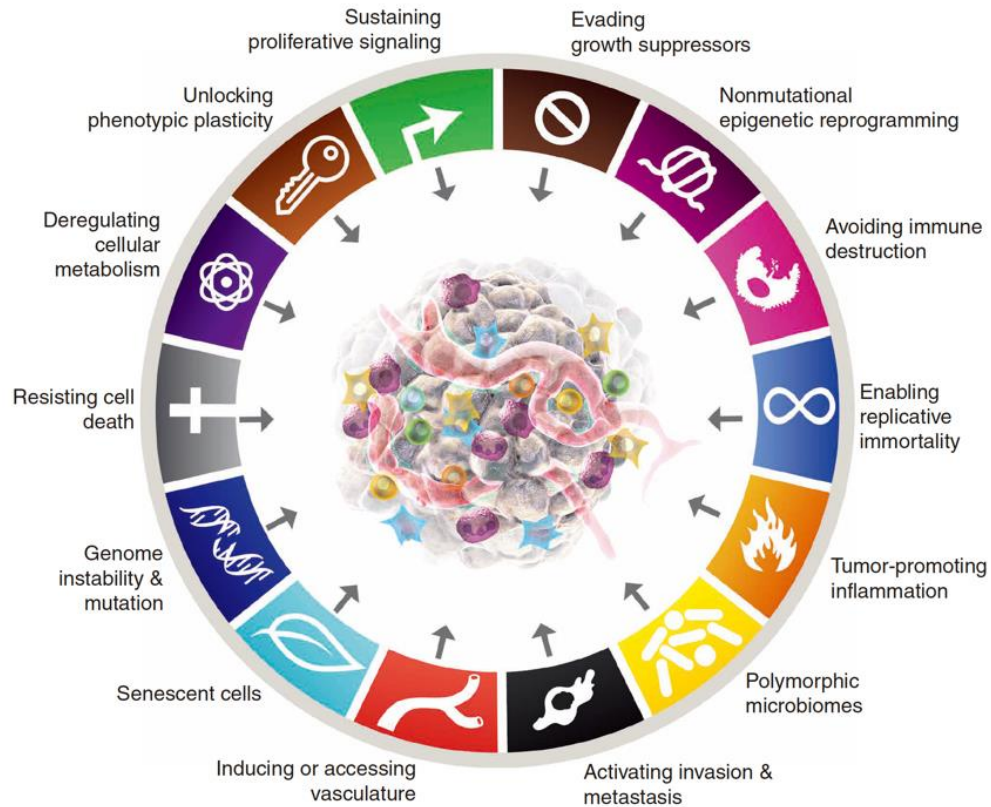


Figure 1. Hallmarks of cancer.

The "Hallmarks of Cancer" constitute a framework outlining fundamental characteristics that cancer cells acquire during their development. Initially proposed by Hanahan and Weinberg in 2000 and updated in 2011, the existing hallmarks include sustaining proliferative signaling, evading growth suppressors, resisting cell death, enabling replicative immortality, inducing angiogenesis, and activating invasion and metastasis. Two emerging hallmarks, which were added in 2011, are the deregulation of cellular energetics and the avoidance of immune destruction. Additionally, enabling characteristics encompass genome instability, mutation, and tumor-promoting inflammation. Figure adapted from (Hanahan 2022).

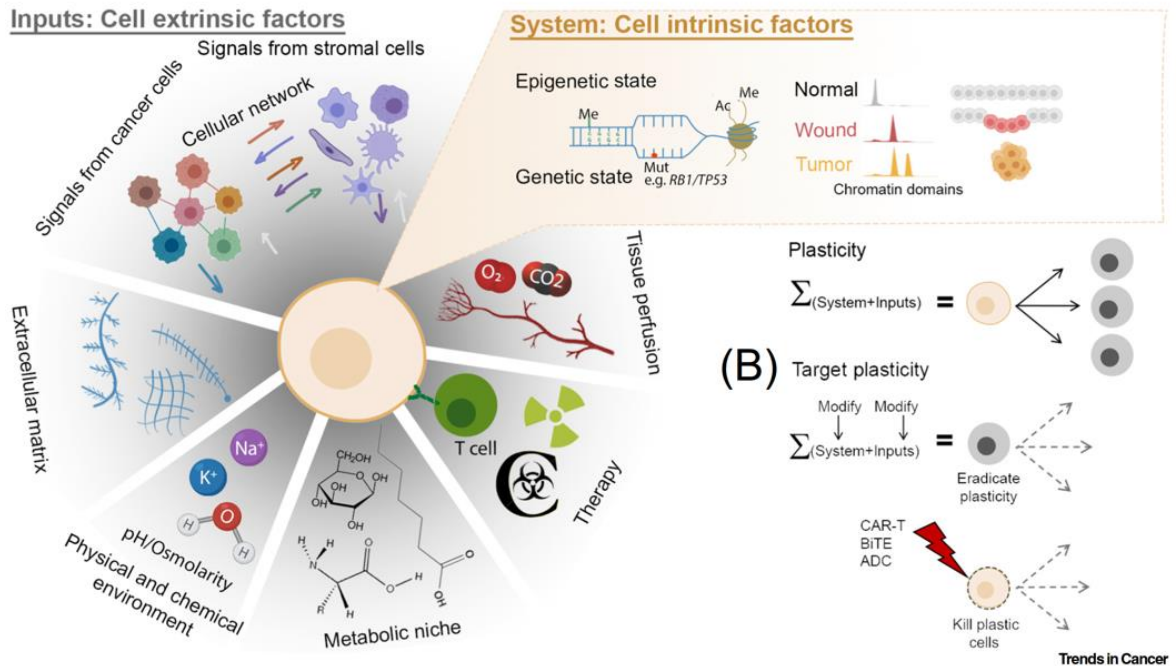


Figure 2. Molecular mechanism of plasticity.

(A) Cellular plasticity results from a combination of internal cellular features (system) and external influences (inputs). Internal features encompass epigenetic mechanisms such as DNA methylation (Me), mutational status (Mut), histone modifications such as acetylation (Ac) and methylation (Me), and differences in chromatin accessibility. Changes in chromatin accessibility linked to processes such as wound healing contribute to increased plasticity and collaborate with tumor initiation. (B) Strategies to target plasticity may involve modifying the system or the inputs responsible for establishing flexible cell states. Alternatively, cytotoxicity can be directed towards highly plastic cancer cells using cell surface markers. Abbreviations include ADC: antibody–drug conjugate; BiTE: bispecific T cell engager; and CAR-T: chimeric antigen receptor T cell. Figure adapted from (Torborg et al., 2022).

4. Current understanding of odontogenic tumors

4.1 Ameloblastoma

Ameloblastoma (AM) is the most commonly encountered and clinically significant odontogenic tumor across all ethnic groups. It constitutes approximately 1% of head and neck neoplasms in Europe and the USA, with the highest incidence observed in Afro-Caribbean populations (Morgan 2011).

Clinical features: The presentation site is frequently the mandible (80%) in the third molar region and is commonly associated with unerupted teeth. AM is usually asymptomatic, with pain caused by superimposed inflammatory changes after infection. According to the 2017 World Health Organization (WHO) classification, AMs are clinically categorized into three main types: conventional, unicystic, and extraosseous/peripheral (Shi et al., 2021). Although it is a slow-growing neoplasm, the conventional type of AM usually infiltrates into adjacent bone marrow, while it may also penetrate the cortex and invade the adjacent muscle and local soft tissues. Hence, marginal or segmental resection remains the mainstay of management for solid AM lesions (McClary et al., 2016). Nevertheless, AM exhibits a notable recurrence rate, historically fluctuating between 5% and 30% within 5 to 15 years. Furthermore, the comprehensive reconstruction of oral tissue is often required after surgical treatment, which remarkably compromises the patient's quality of life and raises healthcare costs (Chang et al., 2020).

Origins: AM is considered to arise from the epithelial cells of the developing tooth (Fig. 3). Although the pathogenesis of AM has been increasingly studied in recent years (Gomes et al., 2010), the origin of the neoplastic epithelium has remained unknown. Suggestions have proposed that AM may originate directly from the enamel organ during tooth development,

from remnants of the odontogenic epithelium, from the lining of an odontogenic cyst, or potentially even from the basal layer of the oral mucosa. The AM epithelium is likely to derive from the epithelial cells of the developing tooth, given its histological similarity to the tooth germ. Yet, the epithelial rests of Malassez (ERM) cells, the exclusive dental epithelial cells found in adult teeth, have also been regarded as potential tumor initiators (Takeda & Yamamoto 1990).

Histological features: Conventional AM has rather typical features, based on two significant cell populations. The first population is the peripheral basal cells that are often elongated and palisaded and closely resemble the ameloblasts after which it is named. These cells exhibit a reversal of polarity, resembling the shift in the arrangement of nuclei and cytoplasmic organelles seen in their typical developmental counterparts prior to the initiation of enamel matrix secretion. The second characteristic population comprises a multilayered epithelium with relatively few intercellular contacts and a conspicuous extracellular space. Centrally situated and often forming small cysts (microcysts), these cells resemble a layer typically found in the developing enamel organ: the stellate reticulum. The two patterns are follicular and plexiform, yet no evidence suggests distinctions in their natural progression or responsiveness to treatment. Indeed, numerous AMs exhibit a combination of both patterns in varying proportions. The AM stroma lacks distinctive features; thus, these neoplasms are solely as epithelial. The enlargement of the AM means that most become increasingly cystic by merging the intra-epithelial microcysts and cystic degeneration in the connective tissue (stromal cysts), particularly in the plexiform variant.

Genetic alterations: The genetic changes underlying the pathogenesis of AM are poorly understood. Several microarray studies have been conducted; however, the results seem

controversial at specific points (DeVilliers et al., 2011, Heikinheimo et al., 2002, Lim et al., 2006). In 2014, three independent groups reported BRAF^{V600E} mutations following the analysis of the AM transcriptome profiles (Brown et al., 2014, Kurppa et al., 2014, Sweeney et al., 2014). The BRAF^{V600E} mutation percentage was up to 63%, 62%, and 46% in each study, respectively, and was the most frequently identified mutation in the AM (mandible). Moreover, SMO showed the highest mutation ratio in maxilla which is up to 39% and 16%. Furthermore, the FGFR2 (18%) and RAS (14%) mutations were also identified with high mutational frequencies. These finding established a new paradigm for the diagnostic classification and clinically actionable drug target for the majority of AM patients (Fig. 4). However, the efficacy of targeted therapies using mutant BRAF and SMO inhibitors is often faced with drug resistance, especially in the case of mutant BRAF-driven tumors, whereby resistance mechanisms often include the compensatory activation of the MAPK kinase pathway (Kim et al., 2013, Menzies & Long 2014). Hence, understanding the comprehensive mechanism of AM development and transcriptomic profiles of individual cells within the AM TME can expedite the exploration and development of alternative treatment approaches.

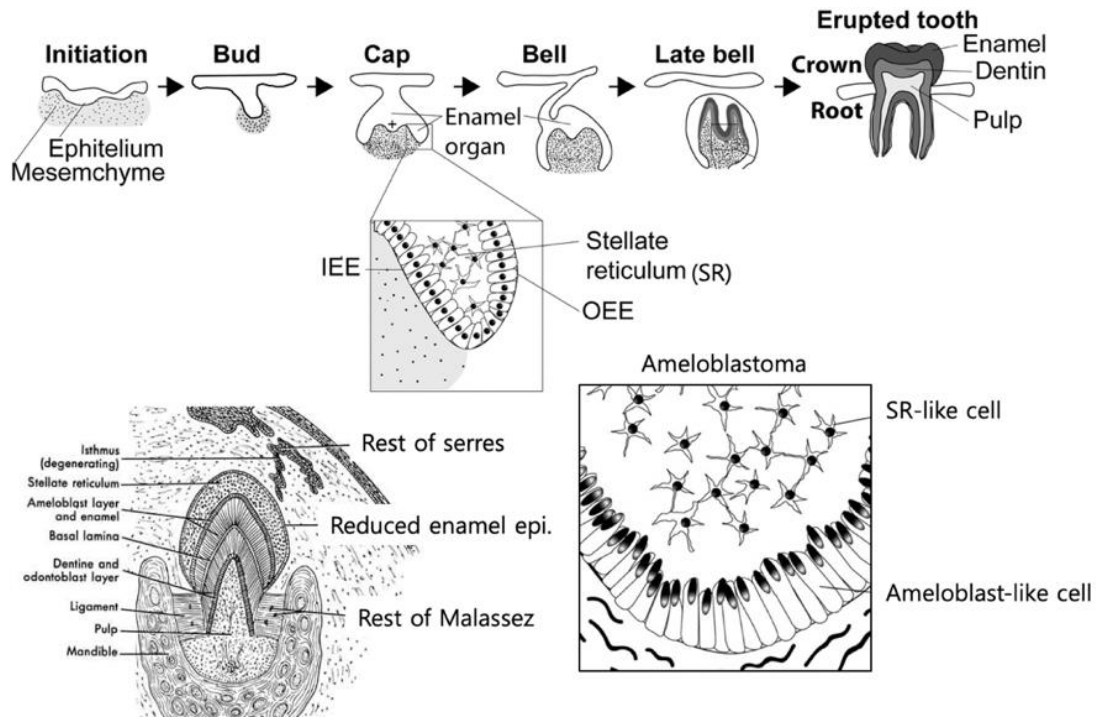


Figure 3. Origin of ameloblastoma.

Schematic illustration of AM histopathologic features that resemble, in part, embryologic patterns seen in the developing tooth. AMs are lesions in the enamel organ and present ameloblast-like cells with reversely polarized nuclei and stellate reticulum-like cells. Figure modified from (Diniz et al., 2017)

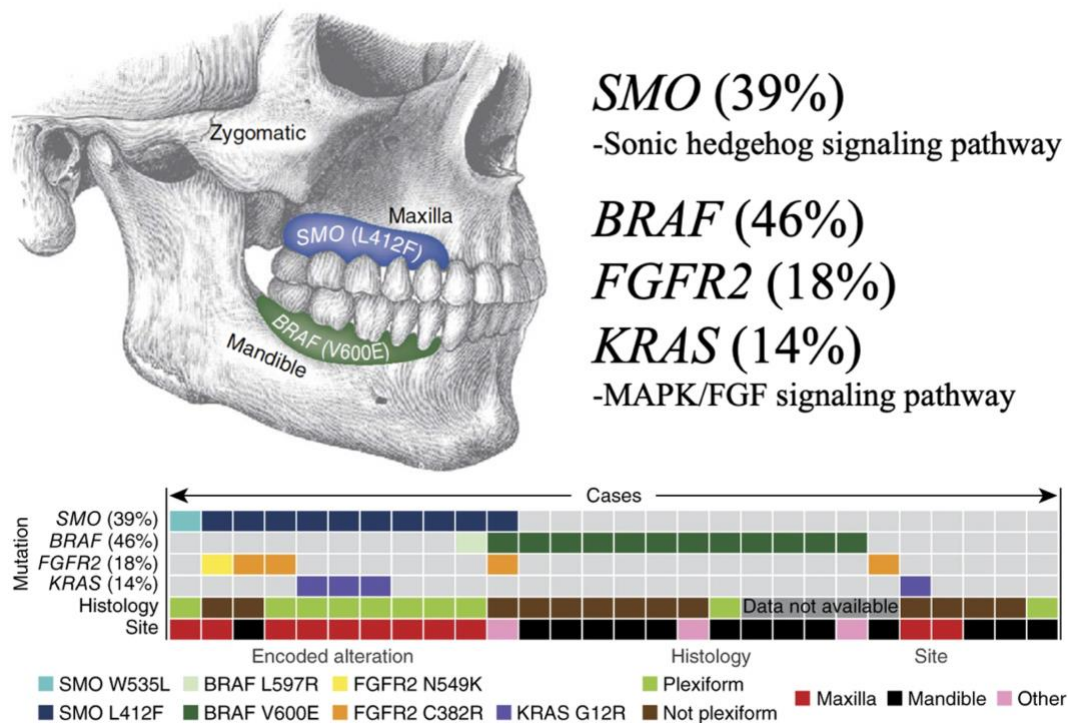


Figure 4. Genetic mutation in ameloblastoma.

Illustration of the spatial distribution of tumors characterized by the identified genetic mutations. The mutation status for four genes is specified, with the overall percentage of cases carrying mutations provided in parentheses. Figure modified from (Sweeney et al., 2014).

4.2 Odontogenic keratocyst

Due to its distinctive feature, odontogenic keratocyst (OKC) has been a significant clinicopathological concern for clinicians; moreover, in contrast to most other odontogenic cysts, it has the potential for a higher recurrence rate even after simple enucleation. Further, the term ‘odontogenic keratocyst’ has been accepted worldwide since the 1950s for this distinctive entity. It was controversially renamed to the keratocystic odontogenic tumor in the 2005 WHO classification; however, in the latest WHO classification, the odontogenic keratocyst terms were returned. The inheritance of this condition follows an autosomal-dominant pattern and is clinically highly suspected in a dental context when odontogenic keratocysts occur in children or manifest as multiple lesions.

Clinical features: In adults or non-syndromic (sporadic) cases, OKC typically manifests without symptoms, appearing as unilocular or multilocular radiolucencies. These cysts do not cause the jaw to expand but instead grow by affecting cancellous bone, winding around the roots of teeth and expanding in the anteroposterior rather than the buccolingual dimension. An OKC occurs across a broad age spectrum, with a predominant presence in the posterior mandible, although occurrence in the lower premolar region or the maxilla is also not uncommon. Smaller radiolucencies often indicate unilocular characteristics. Surgeons are typically the first to suspect an OKC compared to other odontogenic cysts owing to their thin and fragile walls. Indeed, disrupting of the cyst wall can lead to the extrusion of white, semisolid material (keratin) from the lumen.

Histological features: The histopathological features are readily recognizable, even to non-specialists. The cyst wall is thin and consists of collagenous connective tissue, occasionally exhibiting subepithelial hyalinization, but lacking features indicative of

odontogenic mesenchyme. The epithelial lining typically ranges from 8 to 12 layers in thickness, with the basal layer often displaying elongation and palisading, suggesting a reverse polarity similar to the corresponding layer in AMs. Within the prickle zone between the basal and parakeratinizing surface layers typically three to four cells thick, a basaloid orientation is retained before abruptly flattening at the transition point with the parakeratin layer; the latter frequently shows a corrugated profile. Mitotic figures, in a departure from the norm for odontogenic cysts and many benign odontogenic tumors, can be both frequent and suprabasal. The interface between the epithelium and connective tissue is typically flat, with occasional separation of the epithelium at the basement membrane, with a 'budding' pattern observed in certain instances, which is sometimes linked to multiple odontogenic epithelial rests or satellite cysts within the wall.

Genetic alterations: A prior investigation indicated that both syndromic and sporadic OKC harbor mutations in the PTCH gene. Normally, PTCH suppresses genes that promote proliferation, and the detected mutations are akin to those found in basal cell carcinomas (Barreto et al., 2000, Heikinheimo et al., 2015).

5. Aim and objectives

This project aimed to understand the roles of extrinsic factors, specifically the high Ca^{2+} environment and collagen-rich ECM, on cellular plasticity and the influence on the heterogeneity of cancer cell populations within the AM model system. The objectives of the study were as follows:

- 1) To identify the transcriptomic difference between AM and OKC that relating to extrinsic factors.
- 2) Characterize and investigate the roles of novel extrinsic factors in the cellular plasticity of AM.
- 3) Estimate the therapeutic potential for non-surgical treatment of AM.

II. MATERIALS AND METHODS

1. Tissue specimens and processing

1.1 Patient tumor samples

Patients who were diagnosed with primary and not recurrent AM or OKC and underwent surgery at the Department of Oral and Maxillofacial Surgery, Yonsei University Dental Hospital (Seoul, Republic of Korea) between 2019 and 2021 were enrolled in this study. Ethical approval was obtained from the Institutional Review Boards of Yonsei University Health System (YUHS-IRB 2-2018-0050). The patients' written informed consent was provided by all patients enrolled in the study. Specimens from AM (n=8) and OKC (n=8) patients whose diagnoses were confirmed by two independent pathologists, including a board-certified oral and maxillofacial pathologist, were selected. Specimens were separated for the primary cell culture, histological analysis, and RNA sequencing.

1.2 Cell and organoid cultures

AM specimens were digested in a solution of 3mg/ml Collagenase type I (LS004194, Worthington Biochem, USA) and 4mg/ml Dispase[®] II (4942078001, Roche, Germany) for 1 h at 37°C. Single-cell suspensions were obtained by passing the cells through a 40 µm strainer (Falcon, BD Labware, Franklin Lakes, NJ, USA). The primary AM cell was seeded on the 0.1% Gelatin Solution (PCS-999-027, PRIMARY CELL SOLUTIONS, USA) coated 100mm culture dish and added KBM[®]-2 (CC-3103, Lonza, USA) supplemented with KGM[®]-2 SingleQuots[®] (CC-4152, Lonza, USA) culture medium. The established human AM cell line AM-1 (Harada et al., 1998) was cultured in Keratinocyte serum-free medium (KSFM; 10724-011, Gibco, USA) supplemented with 2.5 µg EGF Human Recombinant (10450-013, Gibco, USA), 25 mg Bovine Pituitary Extract (13028-014, Gibco, USA). Human Embryonic

Kidney Cells 293T (HEK293T cells) were cultured in Dulbecco's modified Eagle's medium (DMEM, Invitrogen, USA) supplemented with 10 % fetal bovine serum (FBS, 12484-020, Gibco, USA), and 1% penicillin/streptomycin solution (P/S, 15140-122, Gibco, USA). All the cells were incubated at 37°C in a humidified atmosphere with 5% CO₂ and used for the following investigations.

For organoid culture, the cell pellet was suspended in Matrigel[®] (356234, Corning, USA) and seeded onto 8 well (30118, SPL, South Korea) culture slides at 2x10⁴ cell density as 20µl Matrigel droplet per well. Matrigel was allowed to polymerize for at least 10 mins at 37°C before addition of AM organoid culture media. AM organoid culture medium was based on KBM[®]-2 supplemented with, 1% N2 (17502001, Gibco, USA), 2% B27 (17504044, Gibco, USA). The following cytokines were added to the medium: Wnt-CM 5mL, 200 ng/mL R-spondin-1 (4645-RS-025, R&D systems, USA), 200 ng/mL Noggin (120-10C, PeproTech, USA), 100 ng/mL EGF (AF-100-15, PeproTech, USA), 100ng/mL FGF10 (345-FG, R&D systems, USA), 10 µM/L Y-27632 (1254, Tocris, USA), 0.5 µM/L A83-01 (909910-43-6, Sigma, USA), 1 mM N-acetylcysteine (A7250, Sigma, USA), 10mM/L Nicotinamide (N0636, Sigma, USA). Growth media was changed every 2 days. Organoid passing was performed by gently disrupting the Matrigel[®] and collecting the organoid suspension in cold KBM[®]-2 supplemented with 1% P/S, HEPES (15630106, Gibco, USA), and GlutaMAX[™] (35050061, Gibco, USA). Organoids were spun down at 204xg for 5 minutes at 4 °C. Medium was aspirated and organoids were resuspended in TrypLE[™] (12604021, Gibco, USA) and incubated for 10 min at 37 °C in a water bath. Subsequently, organoids were disrupted by pipetting up and down with a 1% BSA coated-Pasteur pipette, at least 20 times until the large organoids were disrupted to clumps of cells and/or single cells. TrypLE[™] was

inactivated and washed with KBM®-2. The cell pellet was resuspended in Matrigel® at a ratio of 1:9. Primary AM cells were re-plated at 1:4 ratio in 20 µL Matrigel® drops on pre-warmed 8 well plate.

1.3 Construction of pCDH-CACNA1C overexpression vector

The human CACNA1C cDNA were purchase from Open Biosystems (MHS6278-202857128, Horizon Discovery, UK). Both genes were cloned in pCDH- CMV (#72265, addgene, USA) combined with a cytomegalovirus (CMV) promoter. pCDH-CMV have puromycin for selecting stably transduced cells. All cloning procedures were performed according to the common digestion-ligation protocol. Polymerase chain reaction (PCR) was carried out for three fragments with EcoRI overhanging. Then, all fragments were separately cloned in pCDH-CMV. We verified the pCDH-CMV-CACNA1C construct by digestion and subsequent sequencing. The Cav1.2 overexpression vector was used for lentivirus production.

1.4 Lentivirus production by transfecting HEK 293T cells

Lentiviral production was carried out by transfecting human embryonic kidney 293T cells (HEK 293T) with lentiviral and packaging vectors. For each 100-mm dish, envelope plasmid (VSVG) 5µg, packaging plasmid (Pax2) 10µg and overexpression plasmid (pCDH-CMV-CACNA1C) 10µg and 75µl FuGENE® HD Transfection Reagent (E2311, Promega, USA) were mixed in 10ml OPTI-MEM (31985070, Gibco, USA) and incubated in room temperature for 15min, and then added onto the 70% confluent HEK 293T cells. The medium was changed after 6h into culture medium. The result supernatant was collected 48h, filtered through syringe driven filter Unit 0.45µm (SLHV 033 RS, Millipore, USA). It was used for AM-1 or primary AM transduction.

1.5 Knockdown CACNA1C in AM cells

CACNA1C siRNA was commercially purchased (Santa Cruz, sc-42688, USA), and multiple siRNAs is experimental validated in all cases. Stock siRNA resuspend lyophilized 1000 pmol siRNA in 100 μ L RNase-free water, 10 μ M. Shake for 30 mins at 4 $^{\circ}$ C on a shaking platform. Dilute further to obtain a 2 μ M working stock by taking 20 μ L and mixing with 80 μ L RNase-free water. Aliquot and freeze at -20° C. 3. Negative control siRNA was also purchased in Santa Cruz. 4. siRNA transfection reagent: FuGENE-HD (Promega). For each transfection, dilute 4 μ l of siRNA duplex into 100 μ l OPTI-MEM (solution A); 6 μ l FuGENE-HD were mixed with OPTI-MEM (solution B). And mix gently by pipetting the solution up and down and incubate the mixture for 30min at room temperature. Wash the cells once with 2ml OPTI-MEM, and then add the mixture with 800 μ l OPTI-MEM for each well (35mm) and incubate the AM cells for 6h at 37 $^{\circ}$ C in a CO₂ incubator. After that change to the growth media.

2. Bulk RNA sequencing and analysis

Total RNA was isolated from the three fresh tumor specimens and AM-1 cell line using TRIzol[®] Reagent (#15596-026, Thermo Fisher Scientific, USA) respectively. The RNA was stored at -70° C and measured at an optical density of 260 nm. The mixtures of total RNA were incubated with Oligo dT (Gibco BRL, Rockville, NY, USA). The library was constructed and sequenced using an Illumina HiSeq2500 sequencer (Illumina, CA, USA). Differentially expressed genes (DEGs) between the AM and OKC were identified using the R package for RNA-seq data analysis, DESeq2 (Love et al., 2014). Based on significant DEGs (adjusted p-value < 0.01), gene ontology (GO) analysis was performed using a R package for comparison of biological themes in gene clusters, clusterProfiler (Yu et al., 2012).

The steps were followed as previously described (Kim et al., 2020). The RNA sequencing data have been deposited in the Gene Express Omnibus (GEO) database [GEO: GSE186489].

3. Histology and immunofluorescence

The fresh samples (AM and OKC) or 14-day-cultured tumoroids were immersed in 4% paraformaldehyde (PFA) for fixation. All the paraffin-embedded specimens were sectioned into 5 μm thickness with microtome (RM 2235, Leica, Germany). Picrosirius red and fast green staining followed the conventional protocols. For immunofluorescence staining, the slides were boiled in 10 mM citrate buffer (pH 6.0, 00–5000, Invitrogen, USA) and cooled at room temperature for 20 min. They were mounted on slides coated with poly-L-lysine (Moto Pure Chemicals, Japan) and dried on slide warmer at 37°C overnight. Melt wax on slide at 60°C for 30 min for staining. Then the slides were washing in xylene. Subsequently, the slides were incubated with antibodies against CACNA1C (1:200, Alomone Labs, ACC-003), CK14 (1:500, Abcam, ab7800), CK10 (1:500, Invitrogen, MA5-13705), E-cadherin (1:500, BD Biosciences, AF748), MMP9 (1:200, Merck, AB19016), LGR5 (1:200, Abcam, ab75732), Ki67 (1:200, Abcam, ab16667), PCNA (1:500, Abcam, ab29), NFATc1 (1:200, Santa Cruz, SC-7294), β -catenin (1:500, Santa Cruz, SC-7963), α -smooth muscle actin (α -SMA, 1:500, 14-9760-80, Invitrogen, USA), Vimentin (1:200, #5741, Cell Signaling Technology, USA), Collagen IV (Col IV, 1:200, ab6568, Abcam, UK), Collagen I (Col I, 1:200, Abcam, UK), Snail (1:200, ab63371, Abcam, UK) at 4 °C overnight. Subsequently, the coverslips were washed with PBT, incubated with Alexa Fluor™ 488 Phalloidin (Thermo Fisher, 1:400) and/ or secondary antibodies (Invitrogen, OR, USA) in PBT for 2 h at room temperature, washed again with PBT, were counterstained with TO-PRO™-3 (1:1000, T3605, Invitrogen, USA) in TDW for 15 min. Fluorescence detection was performed

according to the manufacturer's protocols and examined using a confocal laser microscope (DMI8, Leica, Germany).

4. Real-time quantitative polymerase chain reaction (RT-qPCR)

Total RNA was isolated from patients' specimens or confluent primary cell cultures using TRIzol[®] Reagent. The extracted were reverse transcribed using Maxime RT PreMix (#25081, iNtRON, Korea), RT-qPCR was performed using StepOnePlus Real-Time PCR System (Applied BioSystems, USA). The amplification program consisted of 40 cycles of the following: denaturation at 95 °C for 50 seconds, annealing at 61 °C for 30 seconds and extension at 72 °C for 70 seconds. The oligonucleotide RT-qPCR primers for *CACNA1C*, *LGR5*, *CTNNB1*, *MKI67*, *NFATC1*, *WNT3A*, *AXIN2*, *MMP9*, *CCN4*, *LOXL2*, *FAP* and Beta-2-Microglobulin (B2M) are as follows: *CACNA1C* forward: 5'-GCT TAT GGG GCT TTC TTG CAC-3', reverse: 5'-ACT GGA CTG GAT GCC AAA GG-3'; *LGR5* forward: 5'-TAT GCC TTT GGA AAC CTC TC-3', reverse: 5'-CAC CAT TCA GAG TCA GTG TT-3'; *SOX2* forward: 5'-GAG CTT TGC AGG AAG TTT GC-3', reverse: 5'- GCA AGA AGC CTC TCC TTG AA-3'; *KRT10* forward: 5'-AGG GGG CAG TTT CGG AGG TG-3', reverse: 5'- AAG TAG GAA GCC AGG CGG TCA TT -3'; *CTNNB1*-F: 5'-CGC ACC ATG CAG AAT ACG AA-3'; R: 5'-ATC CAC TGG TGA CCC AAG CA-3'; *MKI67*-F: 5'-ACG CCT GGT TAC TAT CAA AAG G-3'; R: 5'- CAG ACC CAT TTA CTT GTG TTG GA-3', *NFATC1*-F: 5'-CAC CGC ATC ACA GGG AAG AC-3'; R: 5'-GCA CAG TCA ATG ACG GCT C-3', *AXIN2*-F: 5'-CCA AGC AGA CGA CGA AGC AT-3'; R: 5'-GTT TCC GGA GCC TTG GAG TG-3', *WNT3A*-F: 5'-CTA CCA GGG AGT CGG CCT TT-3'; R: 5'-AAC TCC CGA GAC ACC ATC CC-3', *MMP9*-F: 5'-CAG TCC ACC CTT GTG CTC-3'; R: 5'-CGA CTC TCC ACG CAT CTC TG-3', *CCN4*-F: 5'-AGT GCT GTA AGA TGT GCG CT-

3'; R: 5'-TGC ACA CAC TCC TAT TGC GT-3', *LOXL2*-F: 5'-ATG TCA CCT GCG AGA ATG GG-3'; R: 5'- TGC TCT GGC TTG TAC GCT TT-3', *FAP*-F: 5'-TGT GCA TTG TCT TAC GCC CT-3'; R: 5'-CTT GTC CTG AAA TCC AGT TTG GAA-3', *B2M* forward: 5'-GCC GTG TGA ACC ATG TGA CT-3', reverse: 5'-GCT TAC ATG TCT CGA TCC CAC TT-3'.

5. Nucleus/cytoplasm fractionation and Western blot

Tissue Nucleus and cytoplasm fractions of AM cells or AM tumoroids were prepared using the NE-PER Nuclear and Cytoplasmic Extraction reagents (Thermo Scientific), following the manufacturer's protocols. The AM-1 or AM cells in protein extraction buffer (RIPA) supplemented with proteinase inhibitor cocktail (cOmplete™; #11697498001, Roche, IN, USA). The whole-cell-lysates or fractionated proteins were separated by SDS-PAGE, transferred to PVDF membranes, blocked with 5% (w/v) skim milk in TBST (10 mM Tris, pH 7.4, 150 mM NaCl, 0.1% Tween 20) for 1 h, and probed with the Rabbit anti-CACNA1C (1:1000, Alomone Labs, ACC-003), mouse anti-PCNA (1:1000, Abcam, ab29), cyclin D1 (1:1000, Santa Cruz, SC-8396), NFATc1 (1:1000, Santa Cruz, SC-7294), β -catenin (1:1000, Santa Cruz, SC-7963), histone H3 (1:1000, Cell Signaling Technology, 3638), GAPDH (1:3000, Santa Cruz, SC-32,233) with gentle shaking at 4 °C overnight. The membranes were washed three times for 15 min each and incubated with HRP-conjugated secondary antibodies for 2h at room temperature. After three washes with TBST, the membranes were developed using the ECL system (RPN2232, GE Healthcare Life Sciences, USA) according to the manufacturer's protocols and visualized by enhanced chemiluminescence (Amersham Biosciences).

6. Intracellular calcium imaging

AM cells were seeded in 35-mm confocal dishes (SPL Life Sciences) at a density of 3×10^6 cells, and the non-adherent cells were removed after 12 h with the KGM®-2 media with DMSO (0.1% v/v), Bay-k8644 (10 nM, 15263, Cayman) or verapamil (VPM, 10 μ M, 1711202, Sigma). The AM cells were washed with HBSS buffer containing Ca^{2+} and Mg^{2+} ions (Gibco), loaded with 5 μ M Fluo-4-AM (Invitrogen) in HBSS buffer containing 0.01% Pluronic F-127 (Invitrogen), and incubated at 37 °C for 30 min. The calcium influx and resting Ca^{2+} levels were measured in the HBSS buffer. Before imaging, cells were washed four times with HBSS buffer. The fluorescence of Fluo-4 was excited at wavelengths of 494 nm every 1 s by means of a high-speed wavelength device. Images were recorded using a Leica DMI8 confocal microscope. To minimize bleaching, the intensity of the excitation light and sampling frequency were kept as low as possible, and 30 cells were analyzed for each experimental condition. The imaging was taken by inverted Laser Confocal Microscope with 0.8 seconds intervals for 140 frames.

7. Organoid-forming assays

Primary organoids were dissociated to single-cells and seeded at a density of 5×10^3 cells per well in an 8 well plate following the published protocol (Boonekamp et al., 2019). Plates were photographed under the brightfield microscope, and organoids were analyzed using ImageJ. Organoids were marked by the circular function in ImageJ and both number and the average size were calculated. Each condition had a technical duplicate and a biological duplicate. Size 25-infinite, circularity 0.5-1.0 (n=10).

8. Image quantification and statistical analysis

To quantify collagen fiber thickness and the number of CAFs, five square ROIs 275×275 μm were randomly selected in the interstitial matrix regions of each slide. Collagen fiber thicknesses were measured manually using the ImageJ (NIH) software. The number of CAFs was manually counted using the Cell Counter Plugin of ImageJ. To examine the collagen alignment, single slices of Picrosirius red and fast green staining images were randomly selected ($N = 10$). The publicly available ImageJ plugin OrientationJ was used with setting for local orientation (ranges from -90° up to 90°) and coherency (ranges from 0 to 1) of every pixel in the images (Koorman et al., 2022). The collagen alignment was strictly quantified by selecting regions of interest within the ECM that are positioned perpendicular to the tumor mass-ECM border (ROIs; 30×150 μm , collagen bundle angle variability perpendicular to the border). Immunostaining procedures were performed on at least three slides for each group of individual samples (biological replicates), with consistent results. All statistically analyzed data were based on at least three separate experiments, with consistent results. Comparisons between two groups were performed using an unpaired two-tailed t test (GraphPad Prism 8; GraphPad Software, USA). p value < 0.05 was considered statistically significant.

III. SECTION 1: Unraveled roles of Cav1.2 in cell stemness and proliferation

1. Introduction

1.1 Role of calcium signaling in cellular functions

Calcium is essential for cellular activity and plays a prominent role in normal and pathological conditions. Various extracellular signals are transformed into transient increases in intracellular Ca^{2+} concentration. Due to the extensive array of spatial and temporal variations in its intracellular concentrations, the Ca^{2+} signal is perfectly positioned to establish connections between extracellular mechanisms and intracellular modifications. These interactions, in turn, contribute to determining specific cell states. Variability in Ca^{2+} signaling depends on a set of tools that guarantee a temporary increase in the concentration of free cytosolic Ca^{2+} . Thus, an elevation occurs either through the influx of Ca^{2+} from the extracellular space or the release of Ca^{2+} from internal reservoirs, primarily found in the ER and mitochondria. Plasma membrane channels facilitate the influx of Ca^{2+} from the extracellular space, while the release of Ca^{2+} from internal stores is triggered by the activation of Ca^{2+} -release receptor channels on the ER membrane or exchangers within mitochondria. What controls these often complex changes in Ca^{2+} levels in the cytosol and subcellular organelles are known as the instruments of Ca^{2+} homeostasis — Ca^{2+} channels, pumps, and exchangers (Monteith et al., 2017). To achieve a temporary increase in cytosolic Ca^{2+} , pumps and exchangers release Ca^{2+} into the extracellular space, which causes an uptake of Ca^{2+} ions back into the cellular reservoirs.

1.2 Calcium toolkit: channel, exchanger, and pump in CSCs

The maintenance or emergence of a population of CSCs is governed by intrinsic factors and extrinsic signals similar to those from the microenvironment stimulating various receptors. Cancer cells often manipulate or alter this designated set of components, called the Ca^{2+} toolkit. In numerous cancers, there is a restructuring of plasma membrane channels and modifications in Ca^{2+} exchanges and intracellular Ca^{2+} signals, which contribute to the development of a neoplastic phenotype. Changes in the activity and/or expression of these specialized proteins promote increased migratory activity, sustained and uncontrolled cell proliferation, and resistance to apoptotic signals. The identification of the enrichment of Ca^{2+} signaling genes in glioma CSCs, correlated with heightened sensitivity to Ca^{2+} -targeted drugs in these immature cells, has laid the foundation for investigations into the roles of the Ca^{2+} toolkit in CSCs (Wee et al., 2014). Additionally, the observation that Ca^{2+} signaling is the initial pathway altered by epigenetic regulators in the CSCs underscores the pivotal role of Ca^{2+} in CSC function (Wang et al., 2018).

1.3 Voltage-gated calcium channel in CSCs

The voltage-operated channels (VOC) or Cav family includes six types of channels: L-, N-, P-, Q-, R-, and T-type (Wu et al., 1998). These channels necessitate a brief depolarization of the plasma membrane to activate the intrinsic voltage sensor, which leads to the subsequent opening of the pore (Rodriguez-Menchaca et al., 2012). Initially identified in "excitable cells" such as neurons and muscles, these channels are also present in cancer cells, where they play a role in regulating both proliferation and migration. Numerous studies have investigated Ca^{2+} -permeable VOCs, yet it remains uncertain whether CSCs exhibit membrane potentials that activate Ca^{2+} -permeable VOCs. In this respect, CSCs from hepatocellular carcinoma displayed a more depolarized resting membrane potential (-7 mV) relative to normal stem

cells (-23 mV), which was related to a differential expression of the GABAergic receptor subunit (Terrie et al., 2019). Remarkably, the $\alpha 2\delta 1$ subunit of the voltage-gated Ca^{2+} channel, encoded by the CACNA2D1 gene, was identified as a marker for CSCs in hepatocellular carcinoma (Sui et al., 2018). These studies also provided evidence that the expression of this VOC alpha-subunit could be closely associated with CSC resistance to radiotherapy and chemotherapy. Indeed, it was demonstrated that cells expressing the VOC $\alpha 2\delta 1$ subunit in small-cell lung cancer or non-small-cell lung cancer exhibit resistance to chemotherapy and radiotherapy, respectively (Yu et al., 2018). Various types of VOCs have been identified in CSCs and are linked to poor prognosis. For example, the T-type Ca^{2+} channel Cav3.2, was more prevalent in CSCs of glioblastoma (CD133pos) compared to non-CSC tumor cells or normal tissue, and is a central regulator of the CSC population (Singh et al., 2004). Pharmacological inhibition of this channel using mibefradil, a drug currently used for hypertension, or its shRNA-mediated knockdown, effectively reduced the CSC population by promoting CSC differentiation. Notably, mibefradil demonstrated efficacy comparable to temozolomide (standard chemotherapy for glioblastoma) in reducing tumor growth in xenografts and exhibited an additive effect when combined with temozolomide, ultimately, leading to prolonged survival in mice (Omuro et al., 2018). Additionally, the study reported that hypoxia, known to enhance resistance to anticancer therapies, also increased the expression of VOC Cav3.2 in glioblastoma (Zhang et al., 2017). CSC resistance poses a significant challenge in oncology, these findings suggest that combined treatment targeting VOCs could enhance current therapies by preventing a resistant CSC population from re-establishing a tumor, even after a successful initial treatment.

2. Results

2.1 Transcriptome profiling of odontogenic tumors

To characterize the differentially expressed transcriptomes in AM among the other odontogenic tumors, we performed bulk RNA-seq of AM (n=3), AM-1 (n=1) and OKC (n=3). To determine the reproducibility of biological replicates and the contribution of the state to the total variability in gene expression, principal component analysis (PCA) was performed. In both analyses, AM were well grouped, indicating high reproducibility of biological replicates. In addition, AM were clustered away from the OKC and AM-1 indicating their discrepancy. However, there was one exception to this clustering in OKC (Fig. 5). GO analysis revealed that among the upregulated genes, calcium-related GO terms were significantly enriched in AM (Fig. 6A). Among several types of VGCCs, the L-type and P/Q-type genes were upregulated in AM. While the N-type, R-type, and T-type VGCCs showed individual variation within each group (Fig. 7A). The stem cell marker LGR5 was enriched in AM and the expressions of the epidermal differentiation markers, including KRT10, were upregulated in OKC (Fig. 7B). Although the individual difference could be shown within a heatmap, the volcano plot displays significantly higher expression of epidermal differentiation markers in OKC (Fig. 6B). Differences in histopathology and molecular expression between AM and OKC were analyzed in patient-derived samples. Epithelial islands consisting of peripheral columnar cells and stellate reticular-like cells were observed in AM (Fig. 7C). In contrast, a thin, regular lining of parakeratinized stratified squamous epithelium with palisading hyperchromatic basal cells was observed in OKC (Fig. 7D). All the patient-derived AM and OKC samples showed these consistent respective phenotypes. CACNA1C (encoding Cav1.2) was dominantly expressed in the CK14 positive peripheral epithelial cell layer in AM and was rarely observed in the CK14 positive basal cell layer in

OKC (Fig. 7E, F). The terminal differentiation marker CK10 was negatively expressed in AM and intensively expressed in the suprabasal layer of OKC (Fig. 7G, H). Moderate expression of the epithelial and mesenchymal transition (EMT) marker E-cadherin and intensive expression of MMP9 were observed in the peripheral cell layer of AM (Fig. 7I). In contrast, E-cadherin was strongly expressed in the lining epithelium, while MMP9 was negatively expressed in OKC (Fig. 7J). LGR5 was intensively expressed in the peripheral cell layer of AM, whereas it was absent in OKC (Fig. 7K, L). In transcriptome analysis of Wnt signaling-related genes, β -catenin inhibitor, *CTNNBIP1* was downregulated in AM, whereas other Wnt molecules and their transcription factors were upregulated in AM (Fig. 6C). The Wnt signaling transduction molecules such as β -catenin and Axin2 were examined between the AM and OKC samples. Nuclear translocated β -catenin was detected in the peripheral layer of AM but not in OKC (Fig. 7M, N). A strong expression of Axin2 was observed in AM, yet was negative in OKC (Fig. 7O, P). These results indicate that the expression of Cav1.2 is concentrated in the peripheral cell layer facing the connective tissue in the epithelium of AM, consistent with the location showing CSC properties such as stemness maintenance and EMT.

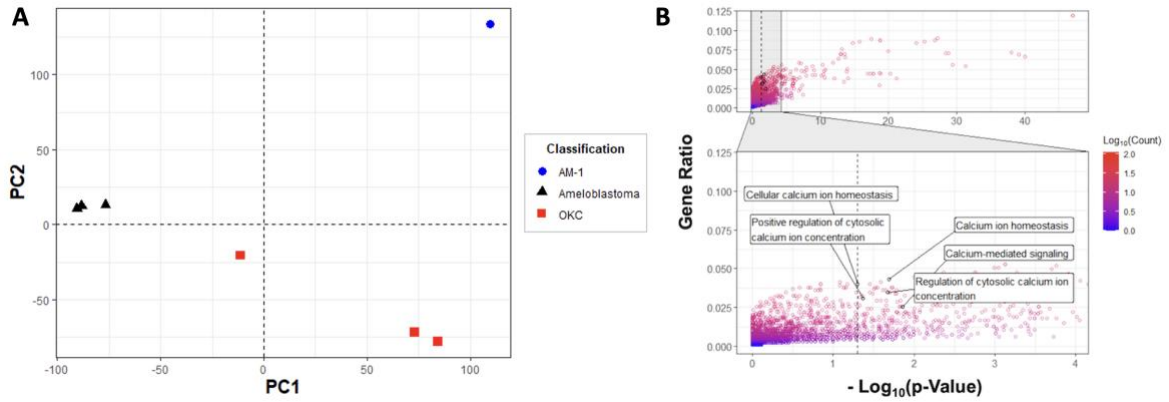


Figure 5. Enrichment of calcium signal-related GO in AM.

(A) Three-dimensional scatter plot of the first three principal components in the data. Each spot represents an RNA-seq sample, and samples with similar transcriptomic profiles are clustered together. The groups are indicated by different colors, as shown in the legend provided. AM specimens (AM, n = 3; black triangle), odontogenic keratocyst (OKC, n = 3; red square), AM cell line-1 (AM-1, n = 1; blue square). (B) Enriched GO terms for upregulated differentially expressed genes (DEGs) in AMs compared with OKCs. Calcium-related GO terms are specifically labeled.

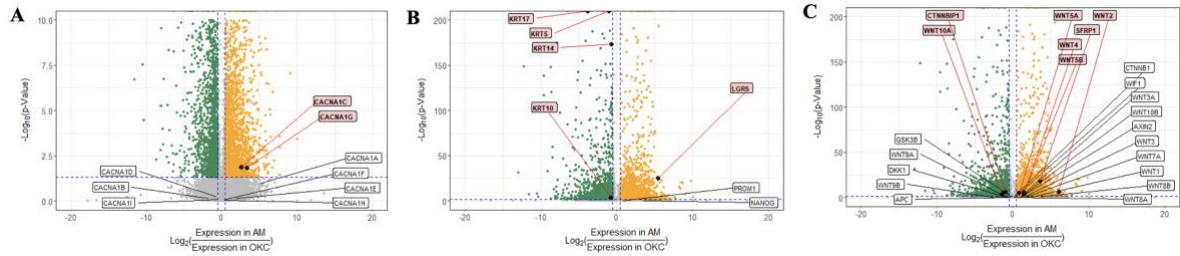


Figure 6. Visualization of differentially expressed genes between AM and OKC

Voltage-gated calcium channels (A), and differentiation and stemness (B), and Wnt signaling-related genes (C) are visualized using a volcano plot. The horizontal dashed line indicates p -values = 0.01, and the vertical dashed lines exhibit fold changes = -2 and 2. Significant genes are indicated by black dots and annotated in pink boxes.

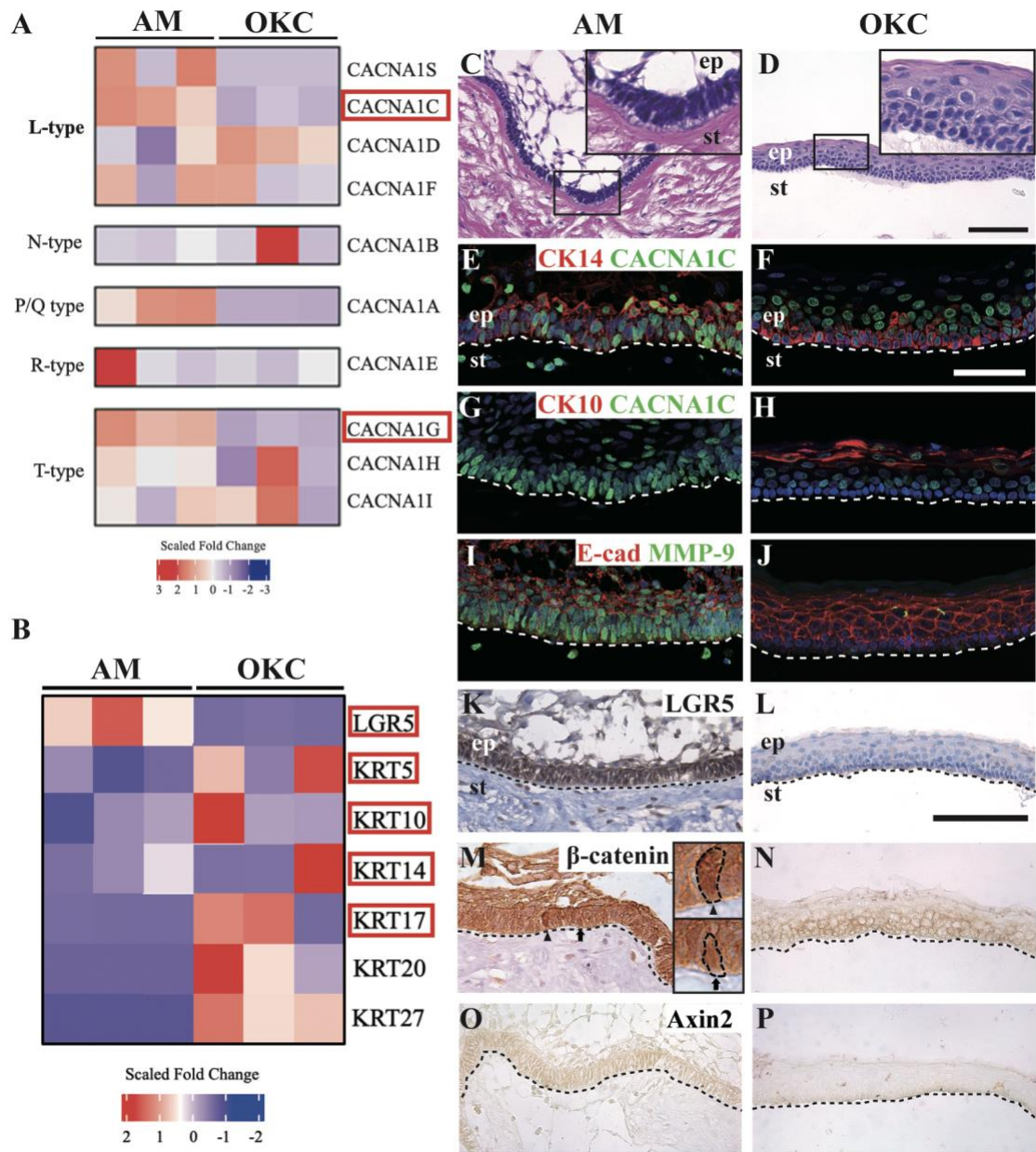


Figure 7. Transcriptomic and histological differences between AM and OKC.

(A, B) Heatmap of differentially expressed genes (DEG) between AM and OKC tissues. Significantly different genes (adj. $p < 0.01$, $|\text{Fold change}| > 2$) are labeled in red boxes. L-type and P/Q-type VGCCs are upregulated in AM, while the N-type, R-type, and T-type VGCCs show a high deviation within the group. LGR5 is enriched in AM, and KRT 5, 10,

14, 17, 20, and 27 are upregulated in OKC. (C, D) Hematoxylin and eosin staining was performed on AM and OKC patient samples. AM epithelial island shows peripheral palisade cells surrounding a central area of stellate-shaped cells. The high-magnification images demonstrate the nuclei displaced away from the basement membrane. The thin, regular lining of parakeratinized stratified squamous epithelium with palisading hyperchromatic basal cells (high magnification) is observed in the OKC sample. (E) In the immunofluorescence staining, CACNA1C is intensely expressed in CK14-positive peripheral cells of AM. (F) Moderate expression of CACNA1C is observed in the CK14-labeled basal layer of OKC. (G) The terminal differentiation marker CK10 is negatively expressed in the CACNA1C positive cell enriched region of AM. (H) Intensive expression of CK10 was observed in the OKC suprabasal cell layer. (I, J) E-cadherin showed moderate expression in AM, and intensive expression in OKC. MMP9 shows intensive expression in the basal cell layer of AM and negative expression in OKC. Nuclei were stained with TO-PRO-3 (TP3). (K, L) The stem cell marker LGR5 shows intensive expression in the peripheral cell layer of AM and negative expression in OKC. (M, N) Intense expression of β -catenin and location in nucleus (Arrow and arrowhead) are observed in the peripheral layer of AM and expressed in the adherence junctions in OKC. (O, P) Moderate expression of Axin2 in epithelial tumor mass of AM, which is absent in OKC. The white or black dotted lines represent the interface of the epithelium and mesenchyme tissues. Scale bars: C, D, 100 μm ; E–J: 50 μm ; K–P: 100 μm . Abbreviations: ep: epithelium; st: stroma.

2.2 Cav1.2 is localized in the filopodia tip of patient-derived AM cells

To determine the role of Cav1.2, patient-derived primary AM (pAM) cells and patient derived primary OKC (pOKC) cells were introduced for further analysis. Cav1.2 was localized explicitly at the tips of the filopodia in pAM cells and intently expressed in cytoplasm, yet this was not observed in the pOKC cells (Fig. 8).

2.3 Dynamic Ca^{2+} influx in pAM cells via Cav1.2

To identify the function of the L-type VGCCs in AM progression, the depolarization of pAM cells was confirmed by using Bay-k8644 (10 nM, L-type VGCCs agonist), VPM (10 μ M, L-type VGCCs blocker) or DMSO (negative control). Calcium imaging was performed to evaluate the calcium influx level during depolarization of pAM cells (Fig. 9A). Depolarization was induced by K-gluconate solution (50 mM), and Fluo-4 AM indicated Ca^{2+} transients. The Ca^{2+} response to K-gluconate in the Bay-k8644 treatment group was significantly active and lasted longer than in the DMSO treatment group (Fig. 9C). In contrast, no fluorescence was detected in the VPM treatment group at any time point after depolarization. The F_{max}/F_0 values in the Bay-k8644 group were 2-fold higher than in the DMSO group and 7-fold higher than in the VPM treatment group (Fig. 9C). In addition, differential proliferative properties were observed in the pAM cells in the presence of DMSO, Bay-k8644, and VPM (Fig. 9D). The number of Ki67 positive proliferating cells was dramatically increased in the Bay-k8644 cells and decreased in the VPM treatment group compared to in the DMSO control (Fig. 9E). Based on these results, we can presume that the Ca^{2+} influx that occurs in the pAM cells via Cav1.2 is involved in the acquisition of cellular plasticity, which could trigger the proliferative capacity.

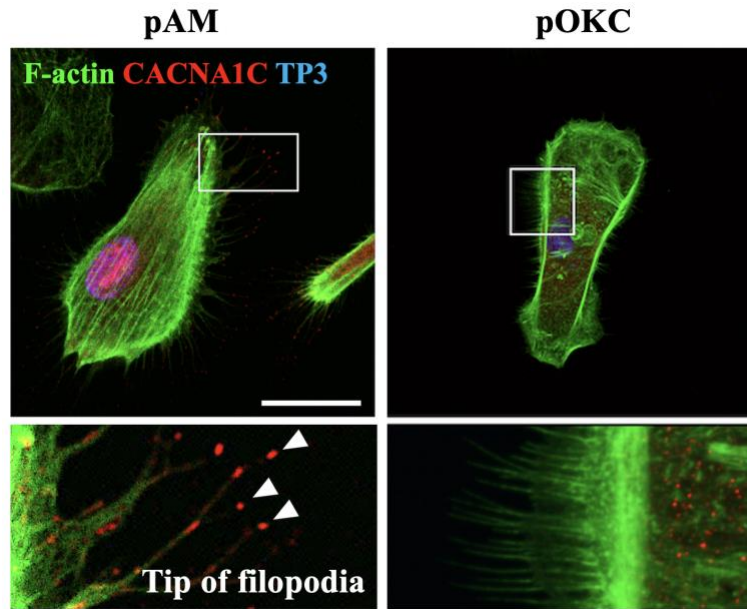


Figure 8. Cav1.2 expression pattern in pAM and pOKC cells.

Immunofluorescence staining of pAM and pOKC cells for F-actin (green) and CACNA1C (Cav1.2, red). Nuclei were counterstained with TO-PRO-3 (TP3, blue). Arrowheads indicate the filopodia tips. Scale bar: 10 μm .

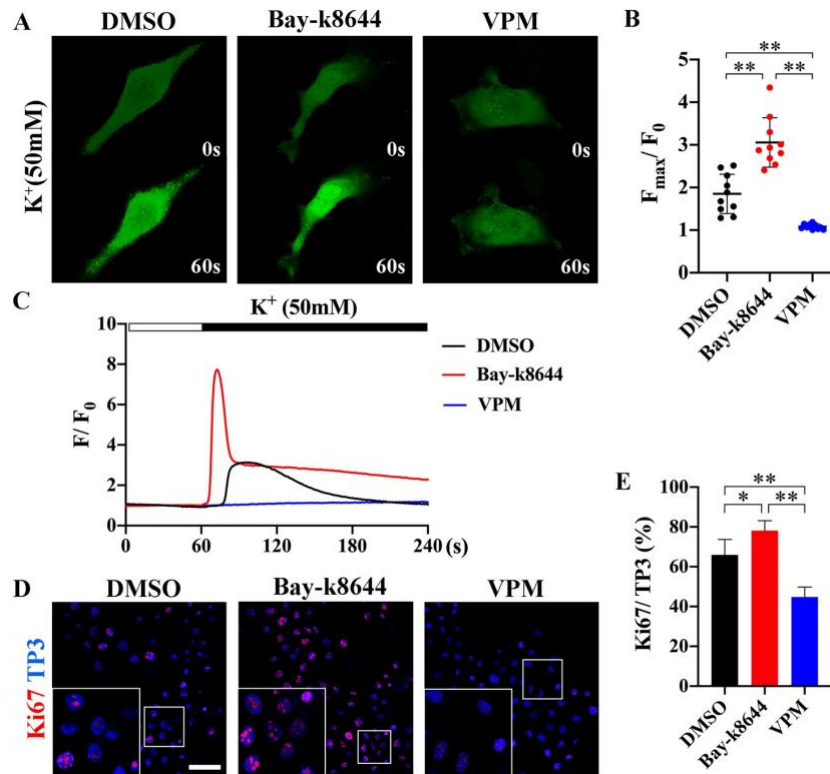


Figure 9. Ca^{2+} influx mediated by L-type VGCC in pAM cells.

(A) Representative image of Ca^{2+} intensity in pAM cells treated with DMSO, Bay-k8644 (10 nM), or VPM (10 μ M). The Ca^{2+} transients are indicated by Fluo-4 AM (green). K-gluconate (50 mM) solutions induced depolarization. (B) F_{max}/F_0 (F_{max} : maximum fluorescence intensity upon stimulation) ratios in the Bay-k8644, DMSO or VPM treatment group (n=10 per group). (C) Ca^{2+} response to K-gluconate in the presence of DMSO, Bay-k8644, or VPM at each time point. Note that the horizontal bar indicates the time of K-gluconate addition. The raw data are expressed as F/F_0 (F: fluorescence intensity; F_0 : mean fluorescence intensity before stimulation). (D) Immunocytochemistry of the proliferation marker Ki67 in primary AM cells with DMSO, Bay-k8644, or VPM. Nuclei were counterstained with TP3. (E) Percentage of Ki67 positive cells (n = 5 per group). Scale bar: 50 μ m. * $p < 0.05$, ** $p < 0.01$.

2.3 Cav1.2-dependent Ca²⁺/NFATc1 signaling coupled with cell proliferation

Several studies have reported that Ca²⁺ signaling is involved in cancer cell proliferation (Kanwar et al., 2020, Monteith et al., 2017, Xie et al., 2017). Therefore, to clarify the role of Cav1.2 in AM cells, we overexpressed or knocked down CACNA1C in AM cells in vitro. CACNA1C was broadly expressed in the cell membrane and nucleus in the CACNA1C overexpression group compared to the vehicle group (Fig. 10A, B). The expression of CACNA1C in the knockdown group was significantly lower than in the scramble control group (Fig. 10C, D). As a Ca²⁺-dependent transcription factor, NFATc1 was primarily found in the cytoplasm. The nuclear accumulation of Cav1.2 detected in CACNA1C-overexpressed AM cells indicates that NFATc1 was activated by Cav1.2 (Fig. 10E, F). NFATc1 expression was dramatically decreased by the inhibition of CACNA1C compared to the scrambled control (Fig. 10G, H). The proliferation marker Ki67 was significantly increased in the overexpression group and decreased in the knockdown group compared to that in the vehicle and scramble groups, respectively (Fig. 10I–L). The percentage of positive cells indicated a correlation between CACNA1C and NFATc1 expression (Fig. 10M). Furthermore, CACNA1C, MKI67, and NFATc1 mRNA expression levels were up-regulated in the overexpression group and down-regulated in the knockdown group (Fig. 10N). In addition, the protein expression of CACNA1C, PCNA, and cyclin D1 was increased in the CACNA1C overexpression group and decreased in the knockdown group compared to the vehicle and scramble groups, respectively (Fig. 10O). The expression level of cytoplasmic NFATc1 was not significantly different between the vehicle and overexpression groups; however, nuclear translocation of NFATc1 was dramatically increased in the overexpression group (Fig. 10P). Cell proliferation was also confirmed using the PCNA expression in the three-dimensionally cultured AM tumoroids (Fig. 11A). PCNA-positive cells were dramatically increased in the

CACNA1C-overexpressed AM tumoroids and significantly decreased in the VPM treatment group (Fig. 11B). We also confirmed that the expression of NFATc1 was up-regulated in the AMs compared to the OKCs, which is consisted with the in vitro results (Fig. 11C). Altogether, Cav1.2-dependent Ca^{2+} /NFATc1 signaling promotes the proliferation of AM cells.

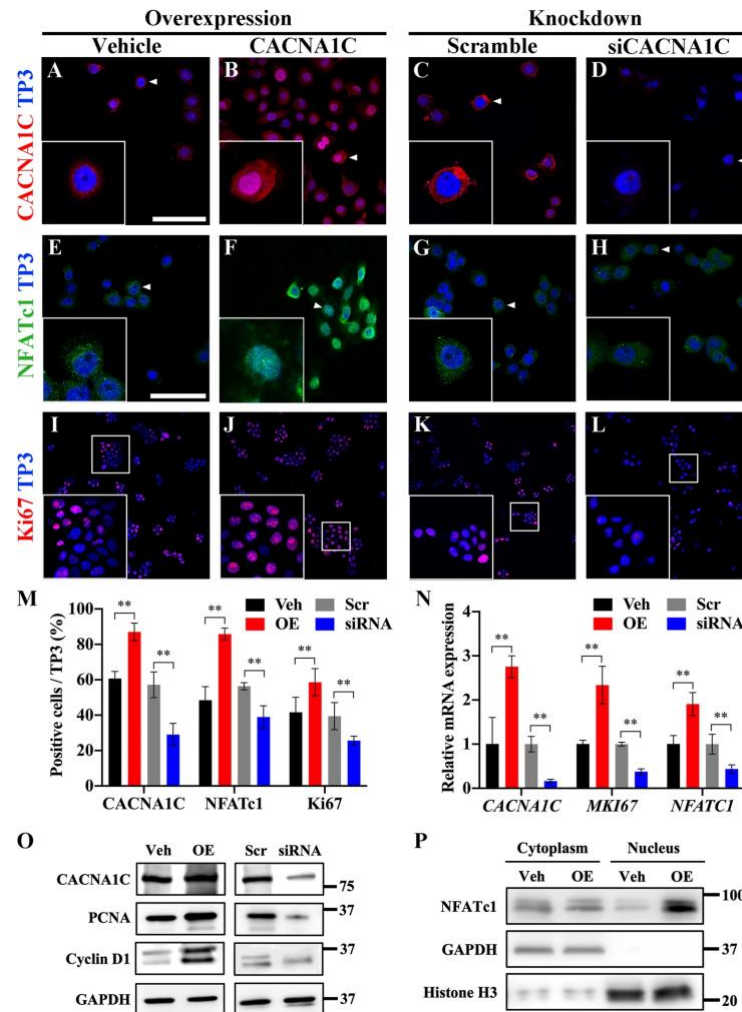


Figure 10. Ca^{2+} influx increased in CACNA1C-overexpressed pAM cells.

(A–L) Representative expressions of CACNA1C, NFATc1 and Ki67 in pAM cells with CACNA1C either overexpressed or knocked down. Nuclei were stained with TP3. Scale bar: 50 μm ; 100 μm . (M, N) Percentages of CACNA1C⁺ and NFATc1⁺ cells (n = 5 per group) and relative mRNA expressions of *CACNA1C*, *MKI67*, and *NFATC1* between vehicle, CACNA1C overexpression, scramble and siRNA group. (O, P) Western blot assay using CACNA1C, PCNA, Cyclin D1, and NFATc1 antibodies. Quantitative data are presented as the mean \pm SD. ** $p < 0.01$. Veh: vehicle; OE: CACNA1C overexpression; Scr: scramble, OE: overexpression.

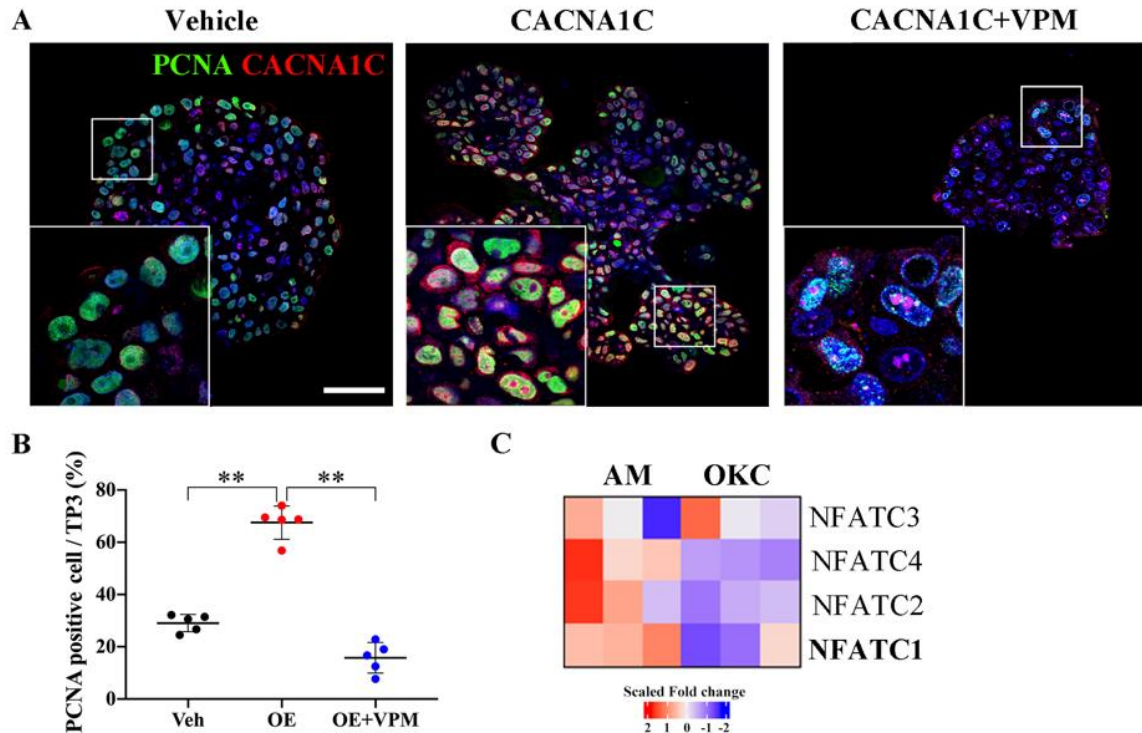


Figure 11. PCNA+ cells increased in CACNA1C-overexpressed pAM tumoroid.

(A, B) Confocal imaging of Ca^{2+} elevation in vehicle and CACNA1C-overexpressed AM tumoroids. The Ca^{2+} transients are indicated by Fluo-4 AM (green), and the depolarization was induced by K-gluconate (50 mM) solutions. Calcium imaging was obtained at 1s intervals for a total duration of 4 min. Scale bar: 25 μm . (C, D) Fluo-4 imaging of the Ca^{2+} response to K-gluconate in the vehicle and CACNA1C-overexpressed AM cells at each time point. Note that the horizontal bar indicates the time of the K-gluconate addition. The raw data are expressed as F/F_0 (F: fluorescence intensity; F_0 : mean fluorescence intensity before stimulation). (E) F_{max}/F_0 (F_{max} : maximum fluorescence intensity upon stimulation) ratios in the Cav1.2-overexpressed group are significantly higher than in the vehicle. Quantitative data are presented as the mean \pm SD. p -value: $**p < 0.01$.

2.4 Function of Cav1.2 in maintaining of Wnt/ β -catenin activity

Three-dimensional (3D) cultures can recapitulate the physiologically relevant phenotypes of the tissue of origin (Qin & Tape 2021). Recently, significant advancements have been made in establishing different organoid or tumoroid models from various organs and cancers, including AM tumoroids (Chang et al., 2020, Kim et al., 2021). CACNA1C overexpressing AM cells were three-dimensionally cultured with the L-type VGCC blocker, VPM. Spherical AM tumoroids were observed in the vehicle group (Fig. 12A), with several budding-like structures extending from the CACNA1C-overexpressed AM tumoroid (Fig. 12B). Then, the budding-like structure reverted in the CACNA1C-overexpressed AM tumoroid in the presence of VPM (Fig. 12C). To evaluate the effect of Cav1.2 on AM cell tumorigenicity, the organoid-forming efficiency was calculated as the number of tumoroids per well (Fig. 12D). With an increase in the number of passages, the organoid formation efficiency in all groups decreased to varying degrees. The vehicle + VPM group and the overexpression + VPM group showed low organoid-forming efficiency from the first passage. The overexpression of CACNA1C effectively retained the organoid-forming efficiency compared to the vehicle or VPM treatment groups. A keratinizing core was observed in the round-shaped tumoroids (Fig. 12E). Budding-like structures were generated from the tumoroid (Fig. 12F) but were dismissed by the addition of VPM (Fig. 12G). The tumoroid size in the overexpression group was significantly increased in both the 14- and 21-day cultures compared to the vehicle and VPM treatment groups (Fig. 12H). Interestingly, the overall tumoroid sizes were very similar between the vehicle + VPM and the overexpression + VPM groups. Furthermore, the dominant expression of the nuclear translocated β -catenin indicated high Wnt/ β -catenin signaling activity in the overexpression group compared to vehicle and

VPM treatment groups (Fig. 12I–K). A previous study reported that pharmacological or genetic inhibition of the T-type calcium channel Cav3.2 in glioblastoma reduced the CSC population by promoting CSC differentiation (Zhang et al., 2017). Similarly, keratinization was predominantly observed in the suprabasal layer, as indicated by the intense expression of CK10 (Fig. 12L). However, CK10 was negatively expressed in CACNA1C-overexpressed AM tumoroids, suggesting that AM cell differentiation was suppressed by increased Cav1.2 (Fig. 12M). The vehicle + VPM and overexpression + VPM groups showed faint CK10 expression (Fig. 12N). Next, a western blot assay was performed to confirm the effect of Cav1.2 on the maintaining Wnt/ β -catenin signaling activity. The nuclear accumulation of β -catenin in the overexpression group was dramatically increased compared to the vehicle and VPM groups (Fig. 12O). Furthermore, the mRNA expression of the canonical Wnt signaling molecules, including *CTNNB1*, *AXIN2* and the Wnt signaling enhancer *LGR5*, was upregulated by CACNA1C overexpression and downregulated by VPM treatment (Fig. 12P). The expression of *WNT3A* was not affected by CACNA1C overexpression but was dramatically reduced by the VPM treatment in both the Veh + VPM and OE + VPM groups. Thus, the expression of Cav1.2 plays an essential role in maintaining the Wnt/ β -catenin signaling activity in AM cells, thereby representing a crucial element for AM cell stemness.

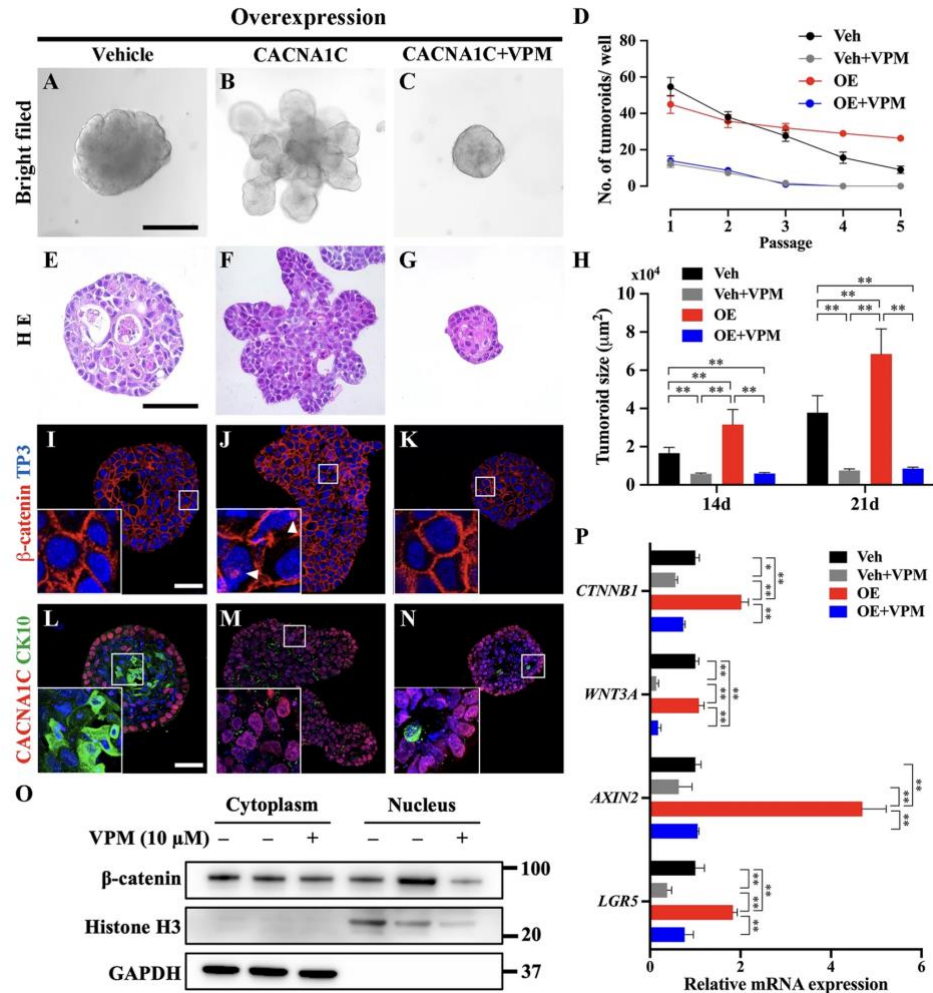


Figure 12. Cav1.2 maintained Wnt/β-catenin signaling activity in pAM tumoroids.

(A–C) Bright-field images of pAM tumoroids. Scale bar: 300 μm. (D) The organoid-forming efficiency was evaluated as a percentage of the tumoroids in each well. (E–G) Hematoxylin and eosin staining of AM tumoroids. Scale bar: 100 μm. (H) Quantification of the size at 14 days and 21 days of culturing AM tumoroids. (I–N) β-catenin, CACNA1C, and CK10 expression in AM tumoroids. Scale bar: 100 μm. (O) Western blot assay for β-catenin. (P) The relative mRNA expression of *WNT3A*, *AXIN2*, *CTNNB1*, and *LGR5* in CACNA1C-overexpressed and VPM-treated tumoroids. Data are presented as the mean ± SD of triplicate experiments. * $p < 0.01$; ** $p < 0.05$. Veh: vehicle; OE: CACNA1C overexpression.

3. Discussion

This present study performed comparative transcriptomic profiling of two representative odontogenic lesions, AM and OKC, for the first time. Remarkably, the L-type and P/Q-type VGCCs were previously observed to be significantly upregulated in AM compared to OKC (Li et al., 2022a). Moreover, various cancers have been associated with the modulation of L-type VGCCs (Kanwar et al., 2020). The expression patterns of CK10, CK14, E-cadherin, MMP9, and LGR5, in this study were consistent with previous studies (Chang et al., 2020, da Silva et al., 2002, Farhan et al., 2022). Interestingly, CACNA1C was co-expressed alongside the general progenitor marker CK14 in AM and was negatively correlated with the terminal differentiation marker CK10 in AM. Furthermore, CACNA1C was positively correlated with MMP9 and LGR5 expression. Our results imply an association between Cav1.2 and the stem/progenitor cell properties. Therefore, any alteration in intracellular Ca²⁺ is important in the capacity of self-renewal, proliferation, and differentiation of stem cells with various Ca²⁺ channels, including VGCCs (Heikinheimo et al., 2015, Tan et al., 2019). The influx of Ca²⁺ increased in the presence of an L-type VGCC agonist (Bay-k8644) in pAM cells *in vitro* and decreased after administering the VPM. Furthermore, according to gain-of-function and loss-of-function studies, AM cell proliferation was positively correlated with both L-type VGCC activity and the expression of Cav1.2. Inactivated NFATc1 can be dephosphorylated by Ca²⁺/calcineurin signaling and translocated to the nucleus, leading to transcriptional activation (Mancini & Toker 2009). Thus, it is known that L-type VGCCs regulate the activity of NFAT in neuronal cells (Graef et al., 1999). Furthermore, the proliferation and anchorage-independent growth of pancreatic tumor cells are dependent on calcineurin activity and high levels of nuclear NFATc1 (Konig et al., 2010). In colorectal cancer progression, calcineurin supported the survival and proliferation of CSCs in an NFAT-

dependent manner (Peuker et al., 2016). The transcriptome analysis results demonstrated a significant upregulation of NFATc1 in AM compared to in OKC (Fig. 14). Without medical treatment, AM generally shows an unlimited growth tendency. Remarkably, we found that CACNA1C positively correlated with NFATc1 expression, as well as an increase in cell proliferation. We also examined the nuclear translocation of NFATc1 in the CACNA1C-overexpressed AM cells. There have been numerous reports on the upregulation of L-type VGCCs in several cancers (Grasset et al., 2018, Jacquemet et al., 2016), including our results, which indicate that Cav1.2-mediated Ca^{2+} influx promotes the nuclear translocation of NFATc1, followed by an increase in AM cell proliferation.

Several studies have shown that the interplay between the calcium channels and the Wnt signaling pathway is critical in maintaining of stem cells. It has been shown that impairment in the activity of the TRPV channels is related to decreased Ca^{2+} flux in bone marrow mesenchymal stem cells, which ultimately downregulates Wnt/ β -catenin signaling, and leads to the dysregulation of the osteogenic differentiation (Liu et al., 2014). Downregulation of Cav1.2 has been shown to induce age-related osteoporosis by suppressing the canonical Wnt signaling pathway (Fei et al., 2019). Ca^{2+} dynamics can finely modulate β -catenin nuclear translocation (Muccioli et al., 2021). Intracellular Ca^{2+} enables β -catenin to pass through the nuclear membrane by neutralizing negatively charged β -catenin and activating Wnt pathway target genes (Thrasivoulou et al., 2013). We have previously shown that activation of Wnt signaling results in the hyper-differentiation of CSCs in AM-1 cells (Kim et al., 2021). Here, the organoid-forming assay showed strong tumorigenicity in Cav1.2-overexpressed AM tumoroids, indicating that Cav1.2 overexpression retains the self-renewal of AM stem/progenitor cells. A similar result was reported, whereby, VGCC knockdown in hepatocellular

carcinoma reduced the self-renewal and tumor formation capacities of CSCs (Zhao et al., 2013). The nuclear accumulation of β -catenin and the upregulation of Wnt signaling molecules in CACNA1C-overexpressed AM tumoroids implies that Cav1.2-dependent intracellular Ca^{2+} plays an essential role in retaining Wnt/ β -catenin signaling activity. In the VPM-treated groups, the tumoroid forming efficiencies, average sizes of tumoroids and even Wnt/ β -catenin signaling activities were almost the same regardless of Cav1.2 overexpression. Additionally, both the VPM treatment groups have a higher degree of differentiation (CK10) than the overexpression group but appear significantly lower than the negative control (vehicle). It indicates that the VPM groups cannot progress to the differentiation stage because tumor progression is suppressed in the tumoroid formation stage. Overall, Cav1.2-dependent Ca^{2+} signaling contributes to the maintenance of AM cell stemness; meanwhile, VPM effectively leads to the retardation of the whole process of tumoroid formation.

In conclusion, we suggest that Cav1.2 regulates NFATc1 nuclear translocation to enhance AM cell proliferation. Furthermore, Cav1.2-dependent Ca^{2+} influx contributes to the Wnt/ β -catenin activity required for the observed AM cell stemness and tumorigenicity. We interpret the effect of calcium-related extrinsic environmental cues on cancer progression as a Cav1.2-mediated Ca^{2+} signal triggering of the AM cell plasticity on proliferation and stem cell properties, which subsequently contributes to tumor heterogeneity in the AM cell population. However, the current study did not explain the underlying mechanism related to Cav1.2-dependent Ca^{2+} signaling, which promotes cell proliferation or enhances the Wnt/ β -catenin activity. Genetic manipulation or pharmacological interventions that target Cav1.2 represents emerging therapeutic possibilities (Li et al., 2022c).

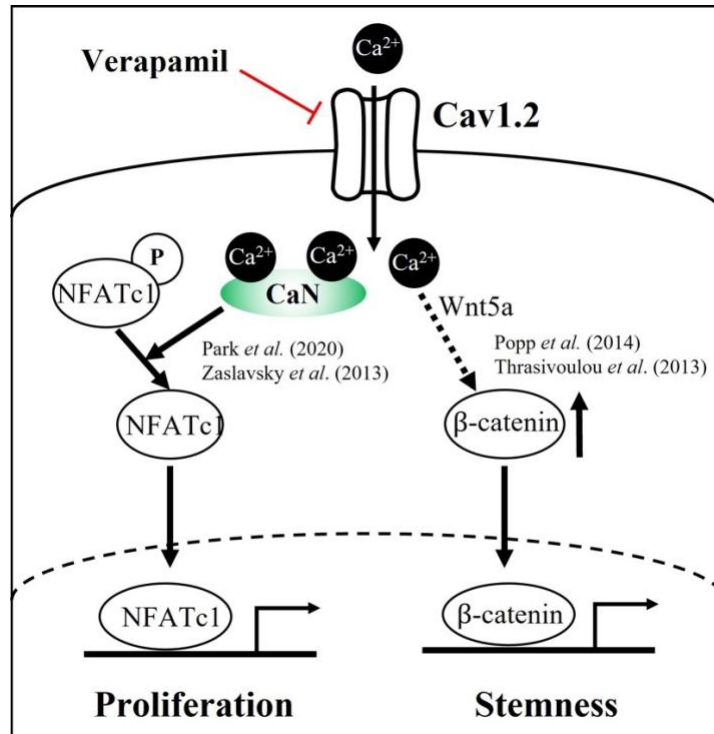


Figure 13. Cav1.2-mediated calcium signaling in AM.

Cav1.2 is dominantly expressed in AM cells compared to OKC. The Cav1.2-dependent Ca^{2+} influx increases the proliferation of AM cells by accumulating nucleic NFATc1, while intracellular Ca^{2+} enhances Wnt/ β -catenin signaling activity via Wnt5 and maintaining the stemness of AM cells.

IV. SECTION 2: Ameloblastoma modifies tumor microenvironment for enhancing invasiveness by altering collagen alignment

1. Introduction

Bidirectional interaction between cells and their microenvironment is essential for maintaining normal tissue homeostasis and facilitating tumor growth (Quail & Joyce 2013). Specifically, the interplay between tumor cells and the surrounding stroma constitutes a significant dynamic that shapes the onset and progression of diseases, ultimately impacting the prognosis of patients (Joyce & Pollard 2009).

The tumor entity comprises a highly heterogeneous cellular component (transformed cell population: cancer cell, CSC; non-transformed cell population: endothelial cell, immune cell, cancer-associated fibroblasts, so-called CAFs), and non-cellular components, such as secreted growth factors, cytokines, and ECM proteins, collectively known as the TME (Poltavets et al., 2018).

The ECM is a major structural component of the TME and is highly dynamic around epithelial tumor mass (Nallanthighal et al., 2019). Collagen is the main component of the ECM, accounting for 90% of the total matrices; thus, it provides not only structural integrity but also determine diverse cellular functions (Gilkes et al., 2014). Dysregulated collagen synthesis and assembly are common driving factors for various pathological conditions. Several secreted molecules involved in ECM remodeling have recently been reported in cancers. WISP1 (CCN4)-induced collagen linearization was found to facilitate breast cancer cell invasion (Jia et al., 2019). High levels of lysyl oxidase enzymes (LOX) were reported to be secreted into the tumor ECM and to crosslink the collagen fibers (Venning et al., 2015). Fibroblast activation protein (FAP) is expressed in various tumor mesenchymal cells and

epithelial cells and enhances tumor cell migration and invasion (Pure & Blomberg 2018). Nevertheless, the interaction between the tumor and the ECM in odontogenic neoplasms arising from a collagen-rich environment, such as the jawbone, remains unclear.

In this study, we used transcriptomic analysis to reveal that ECM remodeling-associated gene expression was augmented in AM compared to OKC, which was verified by an immunohistological assay. Tumoroid analysis indicated that type I collagen is indispensable for AM invasion. More importantly, AM tumoroids remodeled the surrounding ECM via basement membrane degradation and collagen alignment independently of CAFs.

2. Results

2.1 Differences in the tumor microenvironment between AM and OKC

Whole transcriptomic profiles were determined for AM and OKC samples obtained from six individual patients with before GO analysis was performed following a DEG analysis of the raw data. Among the significantly differentially expressed GO terms, TME-related upregulated GOs in AM were categorized into six groups: cell migration, ECM, collagen, ECM component binding, EMT, and MET (mesenchymal-to-epithelial transition). The number of genes in the classified GO terms in each group was counted (Fig. 14a). Genes in the GO groups relating to cell migration, ECM, and collagen were relatively enriched. The expression of genes in the five top-ranked GO terms in the ECM, collagen, and EMT groups are presented as heatmaps and include representative genes such as CCN4, FAP, LOXL2, MMP9, COL1A1, COL4A1, SNAI2, IL6, and TGFB3, which are labeled (Fig. 14b). The heatmaps show a clear separation of the samples into two clusters. However, individual variances were observed among the patient samples, especially in OKC #3, which had a pattern in the entire transcriptomic profile similar to the AMs (Fig. 15a, b). Among the genes

in the GO groups, the primary genes for each category constituting the ECM were selected, and their expression fold changes are presented (Fig. 15c). Altogether, the transcriptomic analysis data revealed that the TME-related genes were significantly upregulated in the AM compared to the OKC.

The distribution of collagen fibers in the surrounding stroma of the AM and the OKC was observed by picrosirius red and fast green staining (Fig. 14c). In the AM, sparse fibers were perpendicularly oriented to the tumor boundary in the region of the basement membrane (black box), and thick bundles of aligned collagen fibers were abundant in the region of the interstitial matrix (blue box). In the OKC, dense bundles of semi-linearized fibers were aligned (pre-aligned) parallelly in the basement membrane region (black box). In contrast, sparse and randomly oriented fibers were observed in the interstitial matrix region (blue box). The thicknesses of the collagen fiber bundles in the interstitial matrix region were significantly higher in the AM than in the OKC (Fig. 14d). In addition, a unique collagen fiber distribution pattern was observed in the tumor-invasive region and non-invasive region of AM (Fig. 20). In the invasive region of AM, thick bundles of aligned fibers were detected in the stroma between the invading strands (Fig. 16a' ①), whereas the fibers were well aligned in the direction that the strand extended (Supplementary Fig. 16a' ②). However, dense and randomly oriented collagen fibers were distributed in the non-invasive region of the AM and OKC stroma (Fig. 16a'', 16b'). The collagen alignment coherency was significantly increased in invasive region of the AM stroma compared to the non-invasive and OKC stroma (Fig. 16c). The majority of CAFs in the AM or OKC samples were localized in the interstitial matrix region, which was indicated by the α -SMA and vimentin double-positive cells (Fig. 14e). The number of CAFs in the AM was significantly higher than in the

OKC (Fig. 14f). Furthermore, a thin and fragmented basement membrane was observed in the AM, whereas a thick and continuous basement membrane was observed in the OKC samples following by Col IV staining (Fig. 14g). MMP9, which is known as a type IV collagenase (Venning et al., 2015), was strongly expressed in the peripheral cell layer of the AM yet was not detected in the OKC (Fig. 14h). Moderate expressions of E-cadherin and Snail-positive cells, known as EMT markers (Kaufhold & Bonavida 2014) were detected in the AM, whereas intense E-cadherin and negative Snail expression patterns were observed in the OKC (Fig. 14i). Overall, these results demonstrate that AM exhibits more basement membrane degradation and EMT properties compared to OKC.

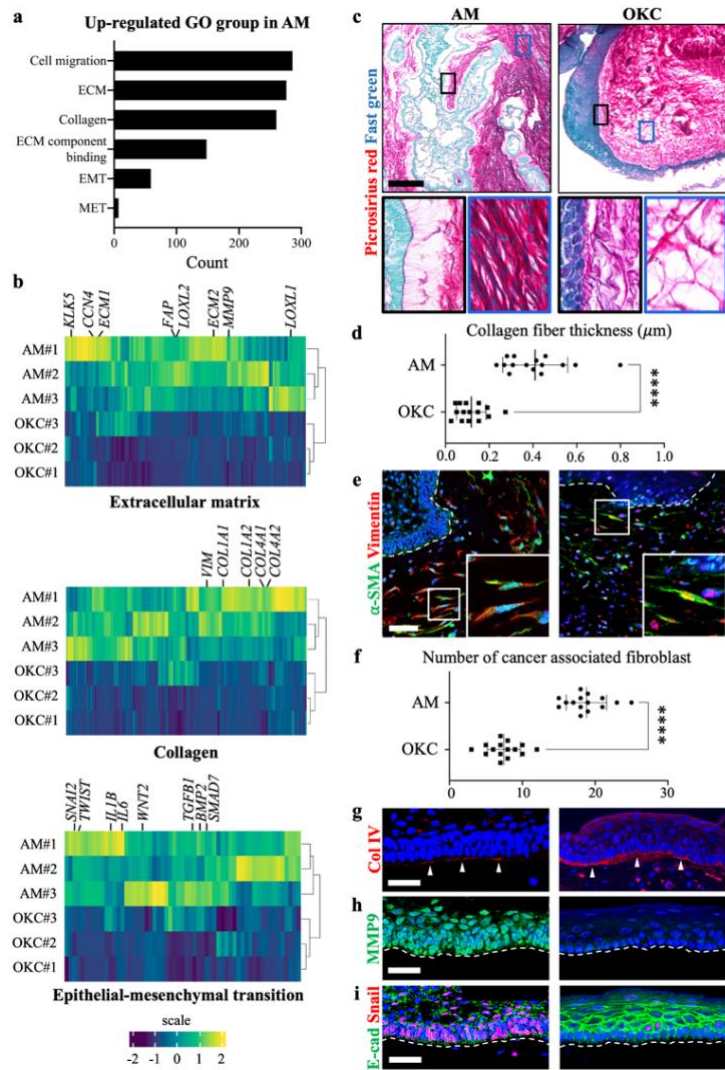


Figure 14. Transcriptomic and histopathologic differences in the TME of AM and OKC.

(a) Upregulated GOs in AM. (b) Heatmaps of the genes related to ECM, collagen, and EMT. (c) Picrosirius red and fast green staining of AM and OKC. (d) Increased thickness of interstitial matrix region collagen fibers in AM compared to the OKC. (e, f) α -SMA and vimentin positive CAFs in AM or OKC. (g–i) Expressions of Col IV, MMP9, E-cadherin and Snail in AM and OKC. The nuclei were stained with TP3. Scale bars: d: 500 μm ; f: 100 μm ; h–j: 50 μm . Quantitative data are presented as means \pm SD. p -value: **** $p < 0.0001$.

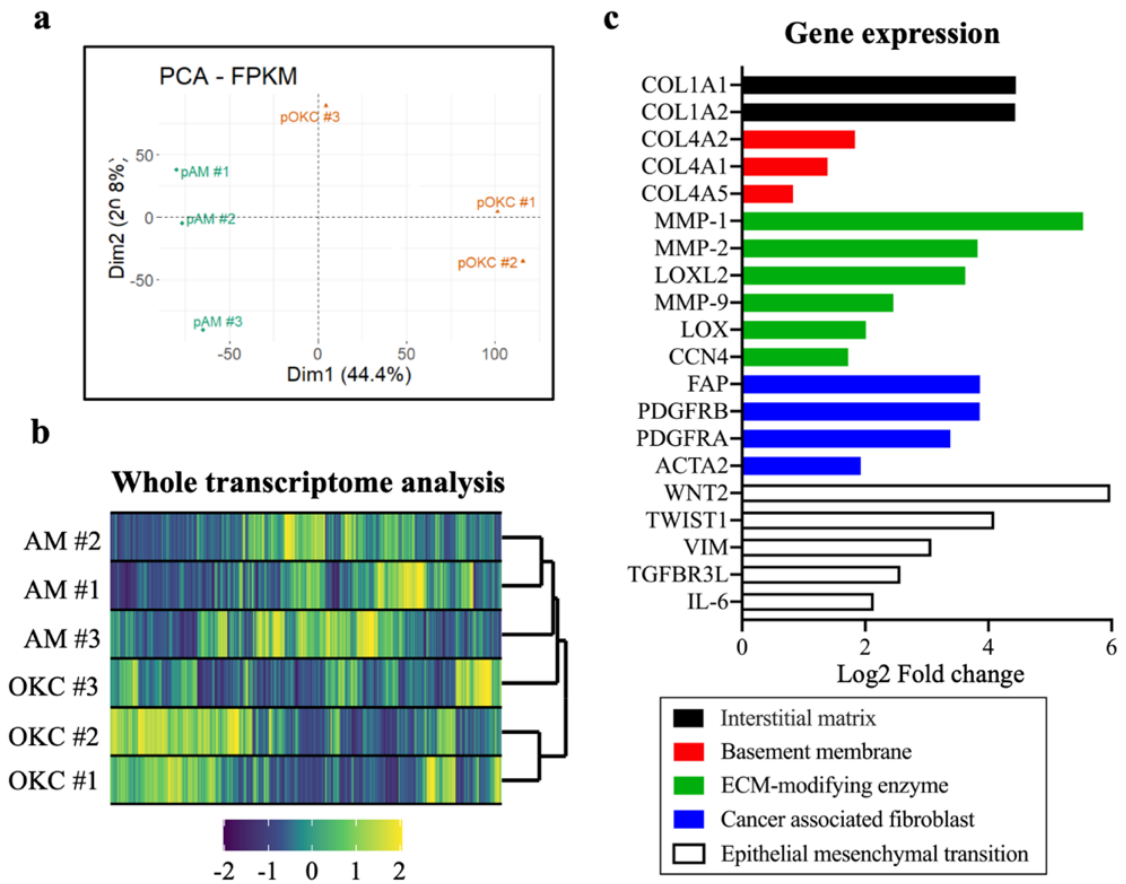


Figure 15. Transcriptomic profiling of AM and OKC.

(a) Principal component analysis (PCA) of the transcriptomes of the AMs and the OKCs. (b) Heatmap of the whole transcriptome showing a significant difference in the transcriptome between the three AM (AM #1, #2, #3) and the three OKC (OKC #1, #2, #3) samples excised from patients. (c) Expression levels of selected major component genes involved in the interstitial matrix, basement membrane, ECM-modifying enzymes, cancer-associated fibroblast, and EMT. All related genes were significantly upregulated in the AM.

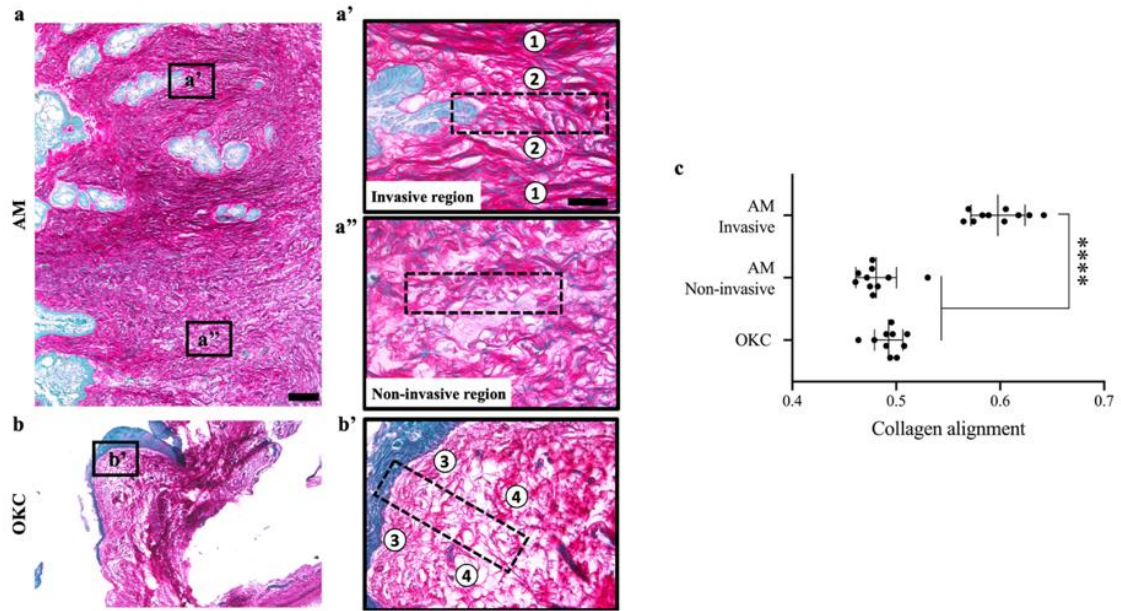


Figure 16. Unique collagen fiber distribution in each stroma of the AM and OKC.

(a and b) Collagen distribution surrounding the AM and OKC tumor mass. (a') Thick, aligned fibers in the stroma between the invading strands (①). Well-aligned fibers in the direction that the strand extended (②). (a'') The collagen fibers in the non-invasive region of AM stroma showed random orientation. (b') Parallely aligned to the basement membrane (③) and randomly distributed (④) wavy collagen fibers distributed in the OKC stroma. (c) Collagen alignment was quantified at the ECM positioned in invasive or non-invasive regions (n = 10). Dotted boxes indicate the regions of interest for alignment quantification. Scale bars: a and b: 200 μm ; a', a'' and b': 50 μm . Quantitative data are presented as the mean \pm SD. *p*-value: **** $p < 0.0001$.

2.2 AM and OKC tumoroid formation in different ECM conditions

Three-dimensional culture can closely recapitulate essential cell–ECM interactions *in vitro* (Micalet et al., 2023). AM and OKC cells isolated from patient samples were cultured in Matrigel[®] or collagen gel for 14 days (Fig. 17a–c). Matrigel[®] provides a connective tissue bed for epithelial cells, including a basal layer, whereas collagen gel can mimic tumor-associated collagen architectures (Gong et al., 2020). Spherical AM or OKC tumoroids were observed in the Matrigel[®] cultures (Fig. 17d, f). In contrast, invading strands were observed in AM tumoroids cultured in collagen gel (Fig. 17e). The OKC failed to form organoids in the collagen gel (data not shown). Collagen I (Col I) was not expressed in the ECM surrounded by Matrigel[®], which was detected at high levels in the collagen gel matrices (Fig. 17g–i). Moderate expression of collagen IV (Col IV) was detected in the fragmented basement membrane of AM tumoroids cultured in Matrigel[®] (Fig. 17g, arrows), while it was also strongly expressed in the continuous basement membrane of OKC tumoroids cultured in Matrigel[®] (Fig. 17i). MMP9, a well-known type IV collagenase, was strongly expressed in AM tumoroids but not in OKC tumoroids (Fig. 17j–l). Radially distributed condensed Col I was also detected at the edge of the invading strand (Fig. 17k, arrowheads). Furthermore, intense expression of E-cadherin was detected in the cell membrane of tumoroids cultured in Matrigel[®] (Fig. 17m, o), whereas it was moderately expressed in AM tumoroids cultured in collagen gel (Fig. 17n). Snail was expressed in the nucleus of the AM tumoroids yet was not expressed in the OKC tumoroids (Fig. 17m–o). In addition, the mRNA expression levels of *MMP9*, *LOXL2*, *CCN4*, and *FAP* were higher in the AM than in the OKC (Fig. 18). In summary, although AM tumoroids retained their aggressive potential, they were not able to invade the ECM without collagen. Furthermore, AM could remodel collagen alignment to a certain degree without CAFs.

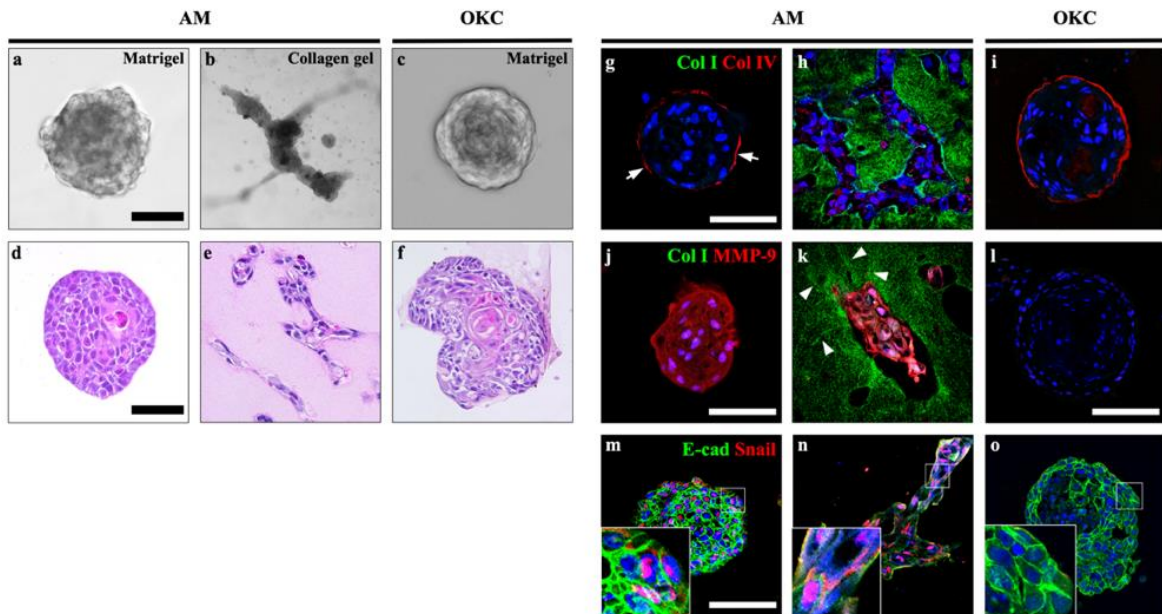


Figure 17. Tumoroid formation by AM and OKC under different ECM conditions.

(a–c) Bright-field images of AM and OKC tumoroids cultured in Matrigel® or collagen gel. (d–f) Hematoxylin and eosin staining of AM and OKC tumoroids cultured in Matrigel® or collagen gel. (g–i) Col I and IV expressions in AM and OKC tumoroids cultured in Matrigel® or collagen gel. Arrows indicates the fragmented basement membrane. (j) MMP9 is broadly expressed in the AM tumoroids. (k) Radially aligned collagen fibers (arrowheads) were indicated by the Col I expression at the edge of the invading strands. Strong expression of MMP9 was broadly expressed in the tumoroid. (l) Col I was not detected and MMP9 was weakly expressed at the basal layer in the OKC tumoroid. (m) E-cad was highly expressed in the cell membrane, and Snail was expressed in the nucleus of the AM tumoroid. (n) Moderate E-cad expression and strong Snail expression in the collagen-cultured AM tumoroid. (o) Snail was not expressed in the OKC tumoroid. The nucleus was counterstained with TO-PRO-3 (blue). Scale bars; a–c: 300 μm ; d–k and m–o: 100 μm ; l: 200 μm .

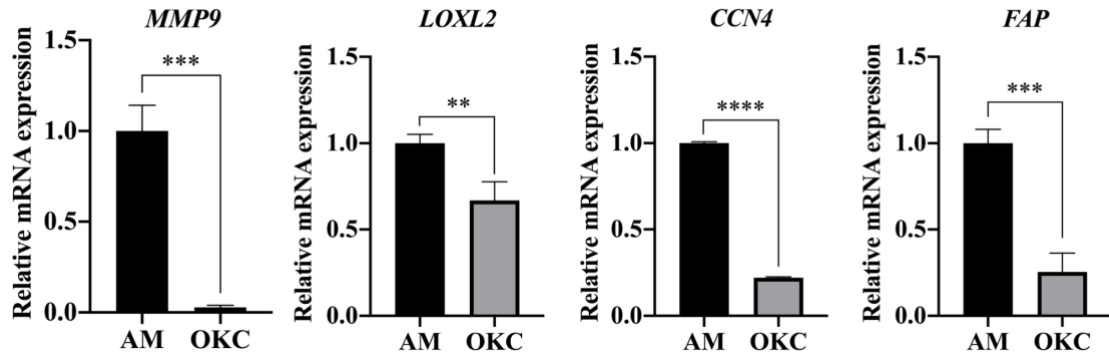


Figure 18. RT-qPCR of secreting collagen remodeling molecules.

RT-qPCR results of MMP9 (type IV collagenase); LOXL2 (lysyl oxidase like-2, generates covalent crosslinks in collagen and elastin resulting in stabilization of ECM); CCN4 (also known as WISP1, a tumor cell-secreted matricellular protein that induces metastatic collagen linearization); FAP (fibroblast activation protein, a serine protease mainly expressed in tissue remodeling site of lesion) upregulation in AM compared to OKC. Quantitative data are presented as the mean \pm SD. *p*-value: ***p* < 0.01, ****p* < 0.001, *****p* < 0.0001.

3. Discussion

In this study, transcriptomic data from AM and OKC patient extracts were generated for the first time and revealed that *MMP9*, *CCN4*, *FAP*, *LOXL2*, *COL1A1*, *COL4A1*, and *SNAI2*, which are involved in ECM, collagen remodeling, and EMT, are upregulated in AM extracts compared to OKC. These findings suggest that AM actively interacts with the surrounding ECM, resulting in aggressive tumor growth compared to OKC.

The ECM comprises a basement membrane and interstitial matrix, which are distinct in function, component, and position. In AM, thin and sparse collagen fibers were observed in the basement membrane region. Therefore, remodeling the basement membrane is essential for cancer cells to invade stromal tissue and form malignant tumors. In contrast, the interstitial matrix region detected thick bundles of aligned collagen fibers. Thus, remodeling of the interstitial matrix in cancer commonly increases the bundling and orientation of collagen fibers, which affects ECM stiffness, cell migration, and tumor progression (Egeblad et al., 2010). This suggests that more active remodeling of the collagen architecture in AM results in more invasive tumor progression than in OKC. α -SMA and vimentin are well-known biomarkers of CAFs (Han et al., 2020). It has been reported that the deposition of excessive collagen-rich ECM by CAFs is essential for tumor progression, and CAFs are the main source of structural ECM in tumors (Sharbeen et al., 2021). Notably, in this study, the number of CAFs in the AM was dramatically higher than in the OKC, which corresponds to the observation of abundant collagen fibers in the AM.

As a gel matrix, Matrigel[®] contains basement membrane (BM) constituents such as laminin, type IV collagen and entactin with a low concentration of type I collagen compared with collagen gel. Several invasive features, including sprouted invading strands and degraded BM, were observed in the AM tumoroids cultured in the collagen gel. Furthermore,

the expression of MMP9 and Snail was significantly higher in the AM than in the OKC tumoroids. These results suggest that invasive growth was impeded without support from type I collagen fibers, although AM tumoroids could degrade the basement membrane through the excessive secretion of MMP9. Remarkably, the collagen gel-cultured AM tumoroids remodeled the surrounding type I collagen into radially aligned and condensed fibers, and the secreted ECM-remodeling molecules known to be present in metastatic tumor tissues were upregulated in the AM tissues. The basement membrane and collagen alignment degradation indicate that AM tumoroids possess the capacity for ECM remodeling, independently of CAFs.

In conclusion, we propose that the ECM remodeling capacity of AM is partially independent of CAFs. A collagen-rich environment contributes significantly to the invasive characteristics of AM, manifesting in heightened MMP9 expression and the secretion of molecules involved in ECM remodeling. This suggests that external factors related to the ECM play a role in prompting cellular plasticity, leading to increased heterogeneity and invasiveness (Fig. 20). To gain deeper insights into the interaction between odontogenic epithelial neoplasms and the surrounding ECM, future studies could explore culturing AM tumoroids with fibroblasts or on a bone matrix (Li et al., 2022b).

Collagen alignment, ECM stiffness, Invasiveness

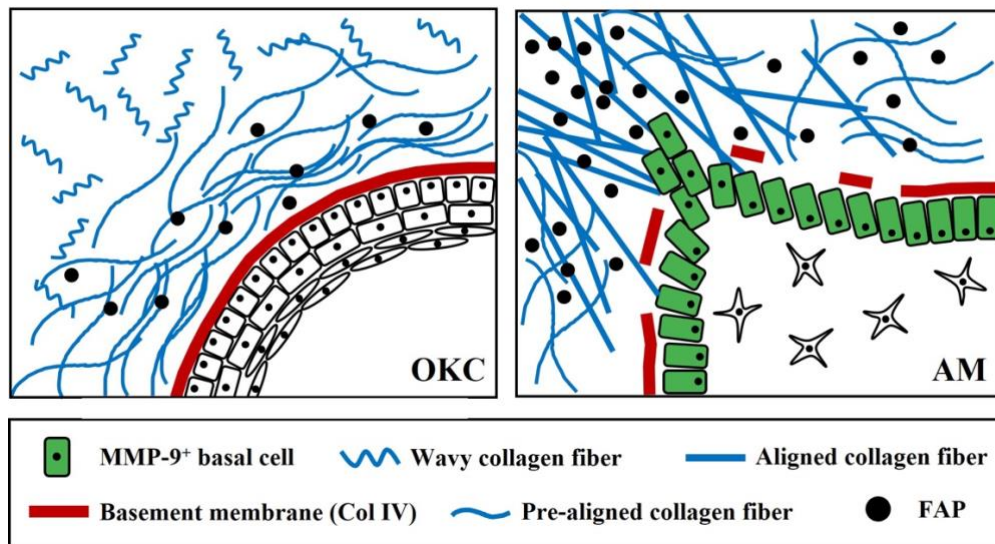


Figure 19. Tumor microenvironments in odontogenic tumors.

The invading strand of AM and lining epithelium of OKC with the surrounding ECM. In AM, basal cells express MMP9 for basement membrane degradation under the invading strand. AM cells secrete fibroblast-associated proteins (FAP) into the ECM. Collagen fibers become bundled and aligned in the direction that the strand extends. In OKC, the basement membrane was entirely continuous, while the epithelium secreted a few FAPs. The pre-aligned collagen fibers near the basement membrane were parallel to the lining epithelium. Thin, wavy, and un-oriented collagen fibers were distributed in the interstitial matrix region. Increased collagen alignment in the AM enhances the stiffness of the ECM and provides a TME for the AM to invade the surrounding tissues readily.

V. CONCLUSIONS AND FUTURE PROSPECTS

1. Conclusions

The present study evaluated the effect of two distinct extrinsic factors, extracellular calcium and the distribution of collagen fibers, on cancer progression from a cellular plasticity perspective. AM was introduced as a model system to study the relationship between TME and cancer cell heterogeneity. The interpretation of the heterogeneity of the AM cell population and the acquisition of plasticity via extracellular inputs (extrinsic factors) are outlined below:

- (1) One prominent characteristic of the TME in AM is the environmentally elevated concentration of calcium ions (Ca^{2+}). As an adaptive response, Cav1.2 (L-type voltage-gated calcium channel) was dominantly expressed in the plasma membrane of AM cells. This intensive, frequent extracellular calcium signaling activated the calcium signal-related transcription factor NFATC1 which contributed to the transition of AM cells to the proliferative state.
- (2) The Cav1.2-mediated calcium signal triggers the nuclei translocation of β -catenin within the non-canonical Wnt signaling pathway. The augmentation of Wnt signaling activity subsequently contributed to the maintenance of cancer stemness, which is essential for establishing intratumoral heterogeneity during the progression of AM.
- (3) The other representative environmental-related feature in AM is the collagen-rich extracellular matrix. The widely distributed, well-aligned collagen bundles constituted a stiffened ECM in the AM and provided a pro-invasive tract for tumor expansion and metastasis. The alignment of collagen fibers functions as an extrinsic factor to provide

the stimulation from extracellular environments for the acquisition of plasticity and, eventually, the attainment of cancer heterogeneity in AM.

2. Future prospects

In addition to its crucial involvement in tumor advancement, cancer cell plasticity plays a significant role in promoting resistance to treatment. It is accomplished by facilitating adaptation to therapeutic pressures by differentiating cells into treatment-resistant states. Researchers and clinicians have gradually realized that more is needed to meet therapeutic objectives than exclusively targeting intrinsic factors (genetic or epigenetic alterations). The extrinsic factors serve as an extracellular input for the cancer cell system, continuously transitioning the cell state to acquire cellular plasticity. Hence, simultaneously tuning the extrinsic factors and intrinsic targets could be a novel therapeutic strategy for comprehensive cancer treatment. Similarly, targeting Cav1.2 or modifying the distribution of collagen fibers in AM (evenly in other cancers that harbored similar environmental cues in the TME) will be a viable option for combination treatments that administer intrinsic factor inhibitors. However, the precise mechanistic network among the interaction between cancer and the surrounding TME and the therapeutic effects on the combined modification of intrinsic and extrinsic factors should be evaluated using a multiple-model system in future studies.

VI. REFERENCE

- Barreto DC, Gomez RS, Bale AE, Boson WL, De Marco L. 2000. PTCH gene mutations in odontogenic keratocysts. *J Dent Res* 79: 1418-22
- Black JC, Atabakhsh E, Kim J, Biette KM, Van Rechem C, et al. 2015. Hypoxia drives transient site-specific copy gain and drug-resistant gene expression. *Genes Dev* 29: 1018-31
- Boonekamp KE, Kretzschmar K, Wiener DJ, Asra P, Derakhshan S, et al. 2019. Long-term expansion and differentiation of adult murine epidermal stem cells in 3D organoid cultures. *P Natl Acad Sci USA* 116: 14630-38
- Brown NA, Rolland D, McHugh JB, Weigelin HC, Zhao L, et al. 2014. Activating FGFR2-RAS-BRAF mutations in ameloblastoma. *Clin Cancer Res* 20: 5517-26
- Chang TH, Shanti RM, Liang Y, Zeng J, Shi S, et al. 2020. LGR5(+) epithelial tumor stem-like cells generate a 3D-organoid model for ameloblastoma. *Cell Death Dis* 11: 338
- Concepcion CP, Ma S, LaFave LM, Bhutkar A, Liu M, et al. 2022. Smarca4 Inactivation Promotes Lineage-Specific Transformation and Early Metastatic Features in the Lung. *Cancer Discov* 12: 562-85
- da Silva MJ, de Sousa SO, Correa L, Carvalhosa AA, De Araujo VC. 2002. Immunohistochemical study of the orthokeratinized odontogenic cyst: a comparison with the odontogenic keratocyst. *Oral Surg Oral Med Oral Pathol Oral Radiol Endod* 94: 732-7
- DeVilliers P, Suggs C, Simmons D, Murrah V, Wright JT. 2011. Microgenomics of ameloblastoma. *J Dent Res* 90: 463-9
- Diniz MG, Gomes CC, de Sousa SF, Xavier GM, Gomez RS. 2017. Oncogenic signalling pathways in benign odontogenic cysts and tumours. *Oral Oncol* 72: 165-73
- Egeblad M, Rasch MG, Weaver VM. 2010. Dynamic interplay between the collagen scaffold and tumor evolution. *Curr Opin Cell Biol* 22: 697-706
- Farhan F, Niazi Z, Masood S, Abbas B. 2022. Immunohistochemical Expression of MMP-9 and E-Cadherin in subtypes of Ameloblastoma. *Pak J Med Sci* 38: 207-13
- Fei D, Zhang Y, Wu J, Zhang H, Liu A, et al. 2019. Ca(v) 1.2 regulates osteogenesis of bone marrow-derived mesenchymal stem cells via canonical Wnt pathway in age-related osteoporosis. *Aging Cell* 18: e12967
- Gilkes DM, Semenza GL, Wirtz D. 2014. Hypoxia and the extracellular matrix: drivers of tumour metastasis. *Nat Rev Cancer* 14: 430-9
- Gomes CC, Duarte AP, Diniz MG, Gomez RS. 2010. Review article: Current concepts of ameloblastoma pathogenesis. *J Oral Pathol Med* 39: 585-91
- Gong X, Kulwatno J, Mills KL. 2020. Rapid fabrication of collagen bundles mimicking tumor-associated collagen architectures. *Acta Biomater* 108: 128-41
- Graef IA, Mermelstein PG, Stankunas K, Neilson JR, Deisseroth K, et al. 1999. L-type calcium channels and GSK-3 regulate the activity of NF-ATc4 in hippocampal neurons. *Nature* 401: 703-8
- Grasset EM, Bertero T, Bozec A, Friard J, Bourget I, et al. 2018. Matrix Stiffening and EGFR Cooperate to Promote the Collective Invasion of Cancer Cells. *Cancer Res* 78: 5229-42
- Han C, Liu T, Yin R. 2020. Biomarkers for cancer-associated fibroblasts. *Biomark Res* 8: 64
- Hanahan D. 2022. Hallmarks of Cancer: New Dimensions. *Cancer Discov* 12: 31-46
- Hanahan D, Coussens LM. 2012. Accessories to the crime: functions of cells recruited to the tumor microenvironment. *Cancer Cell* 21: 309-22
- Hanahan D, Weinberg RA. 2000. The hallmarks of cancer. *Cell* 100: 57-70
- Hanahan D, Weinberg RA. 2011. Hallmarks of cancer: the next generation. *Cell* 144: 646-74
- Harada H, Mitsuyasu T, Nakamura N, Higuchi Y, Toyoshima K, et al. 1998. Establishment of ameloblastoma cell line, AM-1. *J Oral Pathol Med* 27: 207-12

- Heikinheimo K, Jee KJ, Niini T, Aalto Y, Happonen RP, et al. 2002. Gene expression profiling of ameloblastoma and human tooth germ by means of a cDNA microarray. *J Dent Res* 81: 525-30
- Heikinheimo K, Kurppa KJ, Laiho A, Peltonen S, Berdal A, et al. 2015. Early dental epithelial transcription factors distinguish ameloblastoma from keratocystic odontogenic tumor. *J Dent Res* 94: 101-11
- Jacquemet G, Baghirov H, Georgiadou M, Sihto H, Peuhu E, et al. 2016. L-type calcium channels regulate filopodia stability and cancer cell invasion downstream of integrin signalling. *Nat Commun* 7: 13297
- Jia H, Janjanam J, Wu SC, Wang R, Pano G, et al. 2019. The tumor cell-secreted matricellular protein WISP1 drives pro-metastatic collagen linearization. *EMBO J* 38: e101302
- Joyce JA, Pollard JW. 2009. Microenvironmental regulation of metastasis. *Nat Rev Cancer* 9: 239-52
- Kanwar N, Carmine-Simmen K, Nair R, Wang C, Moghadas-Jafari S, et al. 2020. Amplification of a calcium channel subunit CACNG4 increases breast cancer metastasis. *EBioMedicine* 52: 102646
- Kaufhold S, Bonavida B. 2014. Central role of Snail1 in the regulation of EMT and resistance in cancer: a target for therapeutic intervention. *J Exp Clin Cancer Res* 33: 62
- Kim HY, Li S, Lee DJ, Park JH, Muramatsu T, et al. 2021. Activation of Wnt signalling reduces the population of cancer stem cells in ameloblastoma. *Cell Prolif* 54: e13073
- Kim J, Aftab BT, Tang JY, Kim D, Lee AH, et al. 2013. Itraconazole and arsenic trioxide inhibit Hedgehog pathway activation and tumor growth associated with acquired resistance to smoothed antagonists. *Cancer Cell* 23: 23-34
- Kim K, Kang HE, Yook JI, Yu HS, Kim E, et al. 2020. Transcriptional Expression in Human Periodontal Ligament Cells Subjected to Orthodontic Force: An RNA-Sequencing Study. *J Clin Med* 9
- Konig A, Fernandez-Zapico ME, Ellenrieder V. 2010. Primers on molecular pathways--the NFAT transcription pathway in pancreatic cancer. *Pancreatology* 10: 416-22
- Koorman T, Jansen KA, Khalil A, Houghton PD, Visser D, et al. 2022. Spatial collagen stiffening promotes collective breast cancer cell invasion by reinforcing extracellular matrix alignment. *Oncogene* 41: 2458-69
- Kreso A, Dick JE. 2014. Evolution of the cancer stem cell model. *Cell Stem Cell* 14: 275-91
- Kurppa KJ, Caton J, Morgan PR, Ristimaki A, Ruhin B, et al. 2014. High frequency of BRAF V600E mutations in ameloblastoma. *J Pathol* 232: 492-8
- Li S, Kim HY, Lee DJ, Park SH, Otsu K, et al. 2022a. Inhibition of L-type voltage-gated calcium channel-mediated Ca(2+) influx suppresses the collective migration and invasion of ameloblastoma. *Cell Prolif* 55: e13305
- Li S, Lee DJ, Kim HY, Kim JY, Jung YS, Jung HS. 2022b. Ameloblastoma modifies tumor microenvironment for enhancing invasiveness by altering collagen alignment. *Histochem Cell Biol* 158: 595-602
- Li S, Lee DJ, Kim HY, Kim JY, Jung YS, Jung HS. 2022c. Unraveled roles of Cav1.2 in proliferation and stemness of ameloblastoma. *Cell Biosci* 12: 145
- Lih CJ, Harrington RD, Sims DJ, Harper KN, Bouk CH, et al. 2017. Analytical Validation of the Next-Generation Sequencing Assay for a Nationwide Signal-Finding Clinical Trial: Molecular Analysis for Therapy Choice Clinical Trial. *J Mol Diagn* 19: 313-27
- Lim J, Ahn H, Min S, Hong SD, Lee JI, Hong SP. 2006. Oligonucleotide microarray analysis of ameloblastoma compared with dentigerous cyst. *J Oral Pathol Med* 35: 278-85
- Liu Y, Yang R, Liu X, Zhou Y, Qu C, et al. 2014. Hydrogen sulfide maintains mesenchymal stem cell function and bone homeostasis via regulation of Ca(2+) channel sulphydration. *Cell Stem Cell* 15: 66-78

- Love MI, Huber W, Anders S. 2014. Moderated estimation of fold change and dispersion for RNA-seq data with DESeq2. *Genome Biol* 15: 550
- Mancini M, Toker A. 2009. NFAT proteins: emerging roles in cancer progression. *Nat Rev Cancer* 9: 810-20
- McClary AC, West RB, McClary AC, Pollack JR, Fischbein NJ, et al. 2016. Ameloblastoma: a clinical review and trends in management. *Eur Arch Otorhinolaryngol* 273: 1649-61
- McGranahan N, Swanton C. 2015. Biological and therapeutic impact of intratumor heterogeneity in cancer evolution. *Cancer Cell* 27: 15-26
- Menzies AM, Long GV. 2014. Systemic treatment for BRAF-mutant melanoma: where do we go next? *Lancet Oncol* 15: e371-81
- Micalet A, Moeendarbary E, Cheema U. 2023. 3D In Vitro Models for Investigating the Role of Stiffness in Cancer Invasion. *ACS Biomater Sci Eng* 9: 3729-41
- Monteith GR, Prevarskaya N, Roberts-Thomson SJ. 2017. The calcium-cancer signalling nexus. *Nat Rev Cancer* 17: 367-80
- Morgan PR. 2011. Odontogenic tumors: a review. *Periodontol 2000* 57: 160-76
- Muccioli S, Brillo V, Chiericato L, Leanza L, Checchetto V, Costa R. 2021. From Channels to Canonical Wnt Signaling: A Pathological Perspective. *Int J Mol Sci* 22
- Nallanthighal S, Heiserman JP, Cheon DJ. 2019. The Role of the Extracellular Matrix in Cancer Stemness. *Front Cell Dev Biol* 7: 86
- Nowell PC. 1976. The clonal evolution of tumor cell populations. *Science* 194: 23-8
- Omuro A, Beal K, McNeill K, Young RJ, Thomas A, et al. 2018. Multicenter Phase IB Trial of Carboxyamidotriazole Orotate and Temozolomide for Recurrent and Newly Diagnosed Glioblastoma and Other Anaplastic Gliomas. *J Clin Oncol* 36: 1702-09
- Peuker K, Muff S, Wang J, Kunzel S, Bosse E, et al. 2016. Epithelial calcineurin controls microbiota-dependent intestinal tumor development. *Nat Med* 22: 506-15
- Pihan G, Doxsey SJ. 2003. Mutations and aneuploidy: co-conspirators in cancer? *Cancer Cell* 4: 89-94
- Poltavets V, Kochetkova M, Pitson SM, Samuel MS. 2018. The Role of the Extracellular Matrix and Its Molecular and Cellular Regulators in Cancer Cell Plasticity. *Front Oncol* 8: 431
- Pure E, Blomberg R. 2018. Pro-tumorigenic roles of fibroblast activation protein in cancer: back to the basics. *Oncogene* 37: 4343-57
- Qin X, Tape CJ. 2021. Deciphering Organoids: High-Dimensional Analysis of Biomimetic Cultures. *Trends Biotechnol* 39: 774-87
- Quail DF, Joyce JA. 2013. Microenvironmental regulation of tumor progression and metastasis. *Nat Med* 19: 1423-37
- Rodriguez-Menchaca AA, Adney SK, Tang QY, Meng XY, Rosenhouse-Dantsker A, et al. 2012. PIP2 controls voltage-sensor movement and pore opening of Kv channels through the S4-S5 linker. *Proc Natl Acad Sci U S A* 109: E2399-408
- Sharbeen G, McCarroll JA, Akerman A, Kopecky C, Youkhana J, et al. 2021. Cancer-Associated Fibroblasts in Pancreatic Ductal Adenocarcinoma Determine Response to SLC7A11 Inhibition. *Cancer Res* 81: 3461-79
- Shi HA, Ng CWB, Kwa CT, Sim QXC. 2021. Ameloblastoma: A succinct review of the classification, genetic understanding and novel molecular targeted therapies. *Surg-J R Coll Surg E* 19: 238-43
- Singh SK, Hawkins C, Clarke ID, Squire JA, Bayani J, et al. 2004. Identification of human brain tumour initiating cells. *Nature* 432: 396-401

- Sui X, Geng JH, Li YH, Zhu GY, Wang WH. 2018. Calcium channel alpha2delta1 subunit (CACNA2D1) enhances radioresistance in cancer stem-like cells in non-small cell lung cancer cell lines. *Cancer Manag Res* 10: 5009-18
- Sweeney RT, McClary AC, Myers BR, Biscocho J, Neahring L, et al. 2014. Identification of recurrent SMO and BRAF mutations in ameloblastomas. *Nat Genet* 46: 722-5
- Takeda Y, Yamamoto H. 1990. Ameloblastoma located in the alveolar bone: a case report. *J Nihon Univ Sch Dent* 32: 270-4
- Tan YZ, Fei DD, He XN, Dai JM, Xu RC, et al. 2019. L-type voltage-gated calcium channels in stem cells and tissue engineering. *Cell Prolif* 52: e12623
- Terrie E, Coronas V, Constantin B. 2019. Role of the calcium toolkit in cancer stem cells. *Cell Calcium* 80: 141-51
- Thrasivoulou C, Millar M, Ahmed A. 2013. Activation of intracellular calcium by multiple Wnt ligands and translocation of beta-catenin into the nucleus: a convergent model of Wnt/Ca²⁺ and Wnt/beta-catenin pathways. *J Biol Chem* 288: 35651-9
- Torborg SR, Li Z, Chan JE, Tammela T. 2022. Cellular and molecular mechanisms of plasticity in cancer. *Trends Cancer* 8: 735-46
- Venning FA, Wullkopf L, Erler JT. 2015. Targeting ECM Disrupts Cancer Progression. *Front Oncol* 5: 224
- Wang F, Wang AY, Chesnelong C, Yang Y, Nabbi A, et al. 2018. ING5 activity in self-renewal of glioblastoma stem cells via calcium and follicle stimulating hormone pathways. *Oncogene* 37: 286-301
- Wee S, Niklasson M, Marinescu VD, Segerman A, Schmidt L, et al. 2014. Selective calcium sensitivity in immature glioma cancer stem cells. *PLoS One* 9: e115698
- Welch DR. 2016. Tumor Heterogeneity--A 'Contemporary Concept' Founded on Historical Insights and Predictions. *Cancer Res* 76: 4-6
- Widmer DS, Hoek KS, Cheng PF, Eichhoff OM, Biedermann T, et al. 2013. Hypoxia contributes to melanoma heterogeneity by triggering HIF1alpha-dependent phenotype switching. *J Invest Dermatol* 133: 2436-43
- Wu LG, Borst JG, Sakmann B. 1998. R-type Ca²⁺ currents evoke transmitter release at a rat central synapse. *Proc Natl Acad Sci U S A* 95: 4720-5
- Xie R, Xu J, Xiao Y, Wu J, Wan H, et al. 2017. Calcium Promotes Human Gastric Cancer via a Novel Coupling of Calcium-Sensing Receptor and TRPV4 Channel. *Cancer Res* 77: 6499-512
- Yu G, Wang LG, Han Y, He QY. 2012. clusterProfiler: an R package for comparing biological themes among gene clusters. *Omics* 16: 284-7
- Yu J, Wang S, Zhao W, Duan J, Wang Z, et al. 2018. Mechanistic Exploration of Cancer Stem Cell Marker Voltage-Dependent Calcium Channel alpha2delta1 Subunit-mediated Chemotherapy Resistance in Small-Cell Lung Cancer. *Clin Cancer Res* 24: 2148-58
- Zhang Y, Cruickshanks N, Yuan F, Wang B, Pahuski M, et al. 2017. Targetable T-type Calcium Channels Drive Glioblastoma. *Cancer Res* 77: 3479-90
- Zhao W, Wang L, Han H, Jin K, Lin N, et al. 2013. 1B50-1, a mAb raised against recurrent tumor cells, targets liver tumor-initiating cells by binding to the calcium channel alpha2delta1 subunit. *Cancer Cell* 23: 541-56

ABSTRACT IN KOREAN

법랑질 모세포종의 세포 가소성과 이질성에 대한

외인 성 요인의 역할 규명

(지도교수 정한성)

연세대학교 대학원 응용생명과학과

이 서 진

암의 발생과 진행은 종양 내 이질성의 발달과 유지와 함께 가소성의 기본 개념과 밀접하게 연결되어 있다. 특히나 암의 복잡한 특성은 암 집단 내의 이질성으로 인해 항암 치료법의 발전에 어려움을 겪고 있다. 종양 미세환경으로부터 기인된 외인 성 요인은 암세포외부로부터 받는 자극신호로 작용하면서 암의 이질성 형성에 기여하는 세포 가소성의 획득을 위해 세포 상태를 지속적으로 전환시킨다. 법모세포종은 치성 상피 성 종양으로서 종양 미세환경의 외인 성 요인과 암세포의 이질성 사이의 관계를 연구하기 위한 모델 시스템으로 적합하다. 본 연구에서는 법랑질 모세포종 미세환경의 두 가지 전형적인 외인 성 요인(높은 칼슘 이온 환경과 콜라겐이 풍부한 세포 외 기질)의 역할에 관하여 집중적으로 조사했다. Cav1.2 (L-타입 전압 개폐 칼슘 통로)는 법랑질 모세포종 세포의 세포막에서 강하게 발현되었다. 이를 통한 집중적이고 빈번한 세포 외 칼슘 신호 전달은 법랑질

모세포종 세포를 증식 상태로 전환시키는 데 기여하는 칼슘 신호 관련 전사 인자 NFATC1 을 활성화시킨다. Cav1.2 를 통한 칼슘 신호는 비 전형적인 Wnt 신호 전달 경로 내에서 β -catenin 의 핵 전위를 유발한다. Wnt 신호 활성화의 증가는 범랑질 모세포종의 종양 내 이질성 확립에 중요한 암 줄기세포능 유지에 기여한다. 널리 분포되고 일정하게 정렬된 콜라겐 다발은 범랑질 모세포종의 강성이 높은 세포 외 기질을 구성하는데 기여하고 종양의 증식 및 전이를 위한 침습통로를 제공한다. 콜라겐 섬유의 정렬은 세포 가소성을 획득하고 궁극적으로 범랑질 모세포종에서 암 이질성을 확립하기 위해 세포 외 환경으로부터 자극을 제공하는 외인 성 요인으로 간주되기에 충분하다. 따라서 Cav1.2 를 표적으로 삼거나 콜라겐 섬유분포에 대한 조절을 목표로 하는 치료는 (유사한 종양 미세환경을 가지고 있는 다른 암에서도 유사하게 적용될 수 있음) 내인 성 인자 억제제와 함께 암 치료효과를 향상시킬 수 있는 합병치료방법으로 상당한 가능성이 보여진다. 그러나 암세포와 그 주변 미세환경 사이의 상호 작용에 연관된 정확한 메커니즘과 내인 성 및 외인 성 요인을 동시 조절하는 치료방법의 효용성과 실용성은 향후 여러가지 모델 시스템에서 추가 연구 및 평가를 진행 해보아야 할 필요성이 있다.

핵심 되는 말: 세포 가소성; 이질성; 종양 미세환경; Cav1.2; 세포 외 기질; 범랑질 모세포종

PUBLICATION LIST

(*co-first author)

1. Kim HY, Cooley V., Kim EJ, **Li S**, Lee JM, Sheyfer D., Liu WJ, Klein O.D., Joester D., Jung HS. Adult dental epithelial stem cell-derived organoids deposit hydroxylapatite biomineral. *International Journal of Oral Science*. 2023 Dec; 15:55. (IF:14.9)
2. Kim SJ*, **Li S***, Gajendiran M, Jangid AK, Lee DJ, Jung HS, Kim KB. Lipid anchor-mediated NK cell surface engineering for enhanced cancer immunotherapy. *Chemical Engineering Journal*. 2023 Oct; 473, 145211. (IF:15.1)
3. Kim EJ, Kim KH, Kim HY, Lee DJ, **Li S**, Han MN, Jung HS. Harnessing the dental cells derived from human induced pluripotent stem cells for hard tissue engineering. *Journal of Advanced Research*. 2023 Aug; Available online. (IF: 10.7)
4. Kim KH, Kim EJ, Kim HY, **Li S**, Jung HS. Fabrication of functional ameloblasts from hiPSCs for dental application. *Frontiers in Cell and Developmental Biology*. 2023 Jun; 11: 1164811. (IF: 6.684)
5. **Li S**, Lee DJ, Kim HY, Harada H, Jung YS, Jung HS. Transcriptomic Comparison Analysis between Ameloblastoma and AM-1 Cell Line. *International Journal of Stem Cells*. 2022 Nov; 15 (4), 415-42. (IF: 3.011, cover)
6. **Li S**, Lee DJ, Kim HY, Kim JY, Jung YS, Jung HS. Unraveled roles of Cav1.2 in proliferation and stemness of ameloblastoma. *Cell & Bioscience*. 2022 Sep; 12(1):145. (IF: 9.597)
7. **Li S**, Lee DJ, Kim HY, Kim JY, Jung YS, Jung HS. Ameloblastoma modifies tumor microenvironment for enhancing invasiveness by altering collagen alignment. *Histochemistry and cell biology*. 158 (6), 595-602. (IF: 2.531)
8. **Li S**, Kim HY, Lee DJ, Park SH, Otsu K, Harada H, Jung YS, Jung HS. Inhibition of L-type voltage-gated calcium channel-mediated Ca²⁺ influx suppresses the collective migration and invasion of ameloblastoma. *Cell Proliferation*. 2022 Jul; 55 (11), e13305. (IF: 8.755)
9. Chang PE*, **Li S***, Kim HY, Lee DJ, Choi YJ, Jung HS. BBS7-SHH Signaling Activity Regulates Primary Cilia for Periodontal Homeostasis. *Frontiers in Cell and Developmental Biology*. 2021 Dec; 9, 796274. (IF: 6.684)
10. Kim HY, Lee JM, Lee YS, **Li S**, Lee SJ, Bae SC, Jung HS. Runx3 regulates iron metabolism via modulation of BMP signalling. *Cell Proliferation*. 2021 Dec; 54(12), e13138. (IF: 8.755)
11. Kim HY, **Li S**, Lee DJ, Park JH, Muramatsu T, Harada H, Jung YS, Jung HS. Activation of Wnt signalling reduces the population of cancer stem cells in ameloblastoma. *Cell Proliferation*. 2021 Jul; 54(7), e13073. (IF: 8.755)